ADVANCED ELECTRONIC MATERIALS
Open Access
www.advelectronicmat.de

Check for updates

A Comprehensive Guide to Fully Inkjet-Printed IGZO Transistors

Lorenzo Magnarin, Ben Breitung, and Jasmin Aghassi-Hagmann**

In this concise review, the recent advancements in fully inkjet-printed (IJP) indium-gallium-zinc-oxide (IGZO) thin-film transistors (TFTs) over the past years are discussed. IGZO has replaced hydrogenated amorphous silicon (a-Si:H) as the primary channel material for liquid-crystal display TFTs and has gained further attention due to the solution processability of IGZO inks. Despite the longstanding practice of printing IGZO for approximately fifteen years, the realization of fully inkjet-printed devices, including both dielectric and electrode components, represents a recent milestone in research, potentially heralding a cost-effective era for IGZO transistors. In this review, following an introductory exposition of IGZO, the focus is on the different ink formulations, currently deployed for solution-processed IGZO devices, the intricacies of the printing procedure involved are delineated, and ongoing research endeavors pertaining to the printing of dielectrics and electrodes for such devices are expounded upon.

1. Introduction

In recent years, there has been a surge in interest in the exploration of oxide semiconductors, particularly in the realm of amorphous oxide semiconductors (AOS), owing to their significant potential across many applications, especially in display technologies and optoelectronic devices.[1–6] Historically, amorphous silicon (a-Si), typically utilized in its hydrogenated form, has been the predominant choice as a channel material for TFTs[7–10] in displays. However, the escalating demands on TFTs to drive advanced displays, such as OLED-based displays, have outpaced the technological capabilities of a-Si:H (see **Figure** 1a).[3,11] Commencing in 2012, the first displays based on AOS TFTs were introduced, which showed great optical and electrical characteristics (see Figure 1b–d).[12] Among the array of oxide semiconductors, examples include zinc oxide,[13–17] indium zinc oxide (IZO),[18–20] indium tin oxide (ITO),[21] indium oxide[22,23] Notably, IGZO has emerged as a preferred material for displays,[2,12] while ongoing research endeavors explore its potential in other domains such as sensors,[24–27] (non-volatile) memory,[28–30] and memristors for neuromorphic applications.[31–33]

In addition to its high electron mobility, low threshold voltage, and low subthreshold swing, IGZO has demonstrated suitability for flexible TFTs (see Figure 1e).[34] Consequently, the adoption of solution processing techniques of IGZO and amorphous oxide semiconductors, in general, has gained momentum, driven by their lower manufacturing cost,[35] thereby facilitating a broader range of applications for TFT devices. Solution processing methods encompass a range of techniques, including but not limited to inkjet printing,[36–38] spin-coating, chemical bath deposition, and drop-casting.[34,35,39–49] These techniques vary in terms of cost, feature size, tuneability, and maximum substrate size. Inkjet printing of semiconducting materials for TFT channels is a very important aspect of fully solution-processed devices, coupled with research on printing electrodes.[50] Chang's group first paved the way for inkjet printing of amorphous oxide semiconductors in 2005,[45,51] while the first IGZO and indium-zinc-tin-oxide (IZTO) printed layers were also published by Chang's group in 2009.[52,53] This review exclusively centers on one amorphous oxide semiconductor, IGZO, and specifically emphasizes inkjet printing as the fabrication technique of interest, to explore the complexity of such techniques and expand on various processes that surround the inkjet printing of semiconducting metal oxides. Certain experiments have only been conducted utilizing alternative solution processes, such as spin-coating, which makes it necessary to briefly touch upon these alternative fabrication methods to elucidate the primary characteristics of IGZO.

2. Indium-Gallium-Zinc-Oxide

The initial reports on the characterization of indium-gallium-zinc-oxide and the development of IGZO thin-film transistor devices were disseminated in 2003 and 2004 (structure is depicted in **Figure** 2a).[23,34] These seminal studies demonstrated the viability of IGZO as a transparent semiconductor for transistor channels (see Figure 2b), exhibiting relatively large mobilities of

L. Magnarin, B. Breitung, J. Aghassi-Hagmann
Institute of Nanotechnology
Karlsruhe Institute of Technology (KIT)
Kaiserstraße 12, 76131 Karlsruhe, Germany
E-mail: ben.breitung@kit.edu; jasmin.aghassi@kit.edu

The ORCID identification number(s) for the author(s) of this article can be found under https://doi.org/10.1002/aelm.202400478

© 2024 The Author(s). Advanced Electronic Materials published by Wiley-VCH GmbH. This is an open access article under the terms of the Creative Commons Attribution License, which permits use, distribution and reproduction in any medium, provided the original work is properly cited.

DOI: 10.1002/aelm.202400478

 © 2024 The Author(s). Advanced Electronic Materials published by Wiley-VCH GmbH

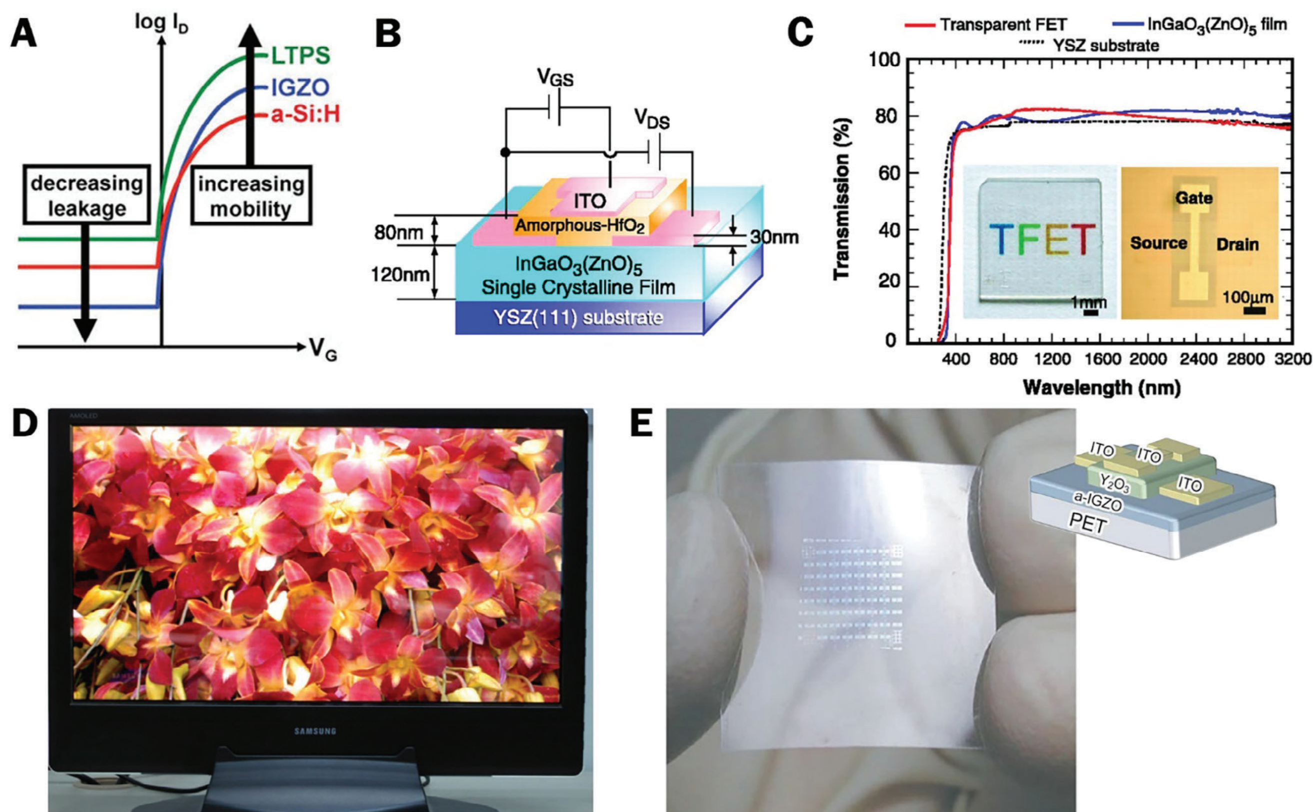

Figure 1. A) Idealized transfer curves of a-Si:H, IGZO and LTPS TFTs. B) TFET device structure with IGZO channel layer and a-HfO_2 dielectric layer. C) Optical transmission spectrum of the in (B) described TFET. D) 19-inch qFHD AMOLED TV with a-IGZO TFT backplane. E) Photograph of flexible TTFT with nested schematic of the devices. (A) Reproduced with permission.[2] Copyright 2014, Wiley. (B,C) Reproduced with permission.[23] Copyright 2003, AAAS. (D) Reproduced with permission.[12] Copyright 2012, Wiley. (E) Reproduced with permission.[34] Copyright 2004, Springer Nature.

7 $cm^2 V^{-1} s^{-1}$ and an on/off ratio exceeding 10^5 (see Figure 2c–e). The salient attribute that renders materials like IGZO noteworthy is their substantial bandgap, endowing them with transparency to visible light. Indium, gallium and zinc atoms bind in such a way that, even in the amorphous phase, the orbitals relevant to the width of the conduction band overlap, enabling high mobilities. The 2p orbitals of the oxygen atoms cause a downward shift of the valence band, effectively enlarging the mobility. This complies with a previous postulate, stating that heavy metal cations possessing an electronic configuration of $(n - 1)d^{10}ns^0$ with $n \geq 4$ represent promising candidates for stable, large bandgap semiconductors with high electron mobilities at room temperature.[54,55] A snapshot taken from the table of elements focusing on these promising candidates can be found in Figure 2f. Building upon these foundational findings, research endeavors focused on IGZO gained momentum, catering to the escalating performance demands of contemporary applications. Subsequent investigations revealed that IGZO channels could achieve mobilities surpassing 10 $cm^2 V^{-1} s^{-1}$, on/off current ratios exceeding 10^7, and enhanced stability to light and voltage bias compared to amorphous silicon, the material it aimed to replace.[3] Furthermore, amorphous IGZO demonstrates n-type behavior, characterized by a carrier concentration (n) exceeding 10^{17} cm^{-3} and a bandgap as high as 3.2 eV.[56] The exceptional properties of IGZO are attributed to its ternary composition, wherein indium, gallium, and zinc contribute distinct properties (see Figure 2g,h).

The principal conduction pathway is facilitated by indium, particularly through the s-states of indium atoms, imparting high conductivity and, consequently, high electron mobility to IGZO.[40,58] While oxides predominantly comprising indium, such as indium oxide and indium-zinc-oxide, also exhibit high electron mobilities, their uniformity and reproducibility are compromised, alongside diminished stability compared to IGZO. This phenomenon in IGZO is ascribed to the effective suppression of oxygen vacancies in the film.[4,58,59] The presence of gallium atoms in the IGZO film, with Ga^{3+} ions demonstrating strong oxygen affinity, accounts for this suppression,[40] affording tunability of carrier concentration by manipulating the gallium molar ratio in the final IGZO film. A study by Shen et al. elucidated the impact of gallium concentration on IGZO films, revealing that elevated gallium concentrations led to diminished carrier mobility and carrier concentration owing to a change in band structure.[60,61] Conversely, the study found that gallium concentration exerted negligible influence on the transparency of the fabricated films. Additionally, the structural stability of the amorphous phase of IGZO is attributed to the presence of zinc atoms within IGZO films.[40,62] Given the significant influence of the constituent elements, numerous studies have investigated the effects of varying the molarity ratios in IGZO channels. One

© 2024 The Author(s). Advanced Electronic Materials published by Wiley-VCH GmbH

2199160x, 0, Downloaded from https://onlinelibrary.wiley.com/doi/10.1002/aelm.202400478 by Karlsruher Institut F., Wiley Online Library on [10/1/2024]. See the Terms and Conditions (https://onlinelibrary.wiley.com/terms-and-conditions) on Wiley Online Library for rules of use; OA articles are governed by the applicable Creative Commons License

2199160x, 0, Downloaded from https://onlinelibrary.wiley.com/doi/10.1002/aelm.202400478 by Karlsruher Institut F., Wiley Online Library on [10/1/2024]. See the Terms and Conditions (https://onlinelibrary.wiley.com/terms-and-conditions) on Wiley Online Library for rules of use; OA articles are governed by the applicable Creative Commons License

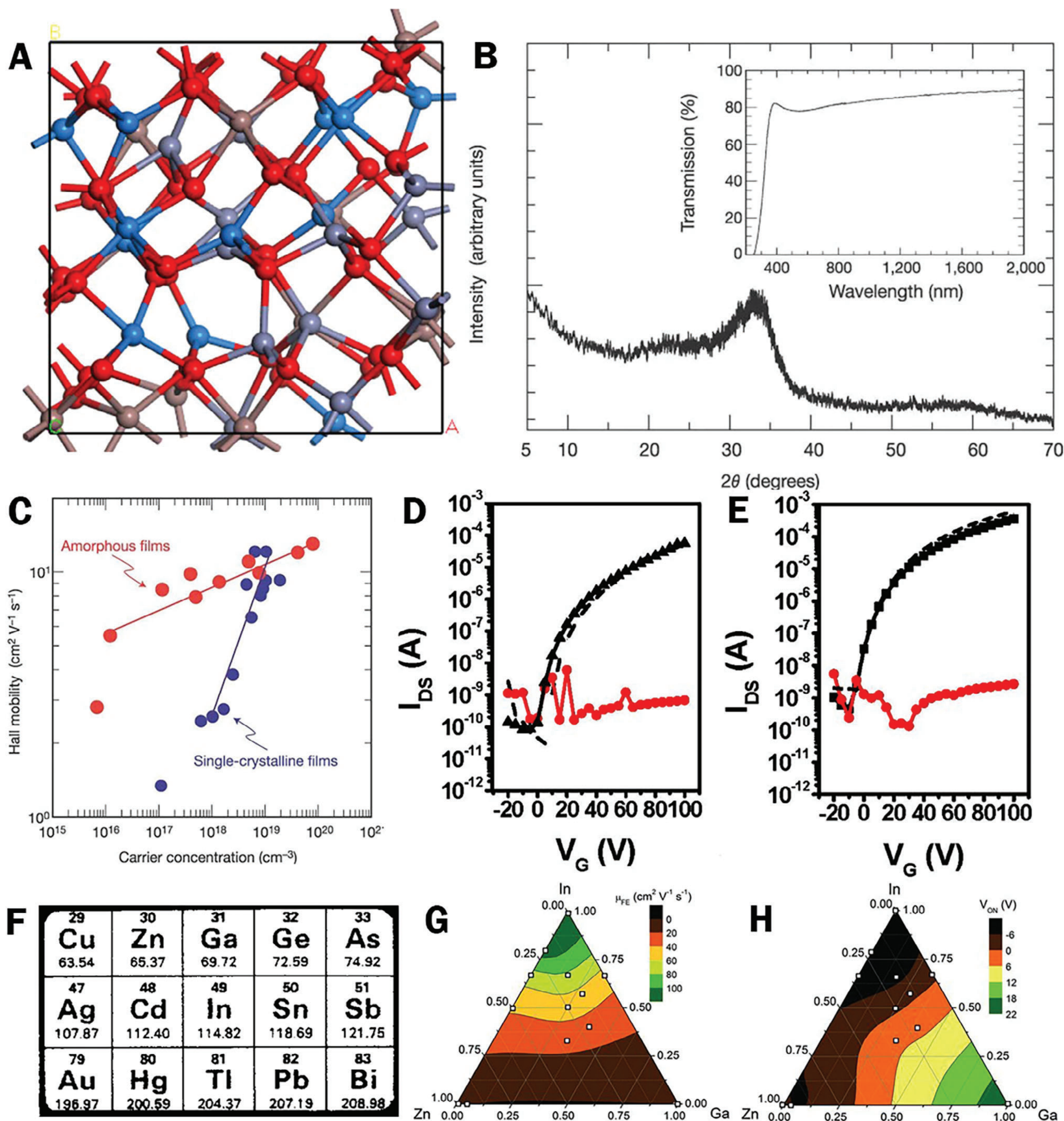

Figure 2. A) Structure of a-IGZO. B) XRD spectrum of a-IGZO films. C) Relation between carrier concentration and hall mobility of amorphous and crystalline IGZO at room temperature. D) Transfer characteristics of back gate top contact (BGTC) IGZO TFTs followed by E) transfer characteristics of back gate back contact (BGBC) IGZO TFTs. The red lines in the transfer curves represent the very low leakage current. F) Candidates' elements for heavy metal cations due to their electronic configuration. G) Visualization of effects of material composition on μ_{FE} and H) V_{ON} of IGZO TFTs. (A) Reproduced with permission.[57] Copyright 2018, American Physical Society. (B,C) Reproduced with permission.[34] Copyright 2004, Springer Nature. (D,E) Reproduced with permission.[40] Copyright 2012, American Chemical Society. (F) Reproduced with permission.[54] Copyright 1996, Elsevier. (G,H) Reproduced with permission.[58] Copyright 2012, Wiley.

 © 2024 The Author(s). Advanced Electronic Materials published by Wiley-VCH GmbH

2199160x, 0, Downloaded from https://onlinelibrary.wiley.com/doi/10.1002/aelm.202400478 by Karlsruher Institut F., Wiley Online Library on [10/1/2024]. See the Terms and Conditions (https://onlinelibrary.wiley.com/terms-and-conditions) on Wiley Online Library for rules of use; OA articles are governed by the applicable Creative Commons License

such study identified the 3:1:1 ratio (In:Ga:Zn) as yielding optimal performance, as evidenced by the transfer characteristics, which exhibited the highest I_{on}/I_{off} ratio.[63] Considering the multitude of parameters influencing the properties of IGZO films, this review endeavors to elucidate the most significant factors, delineating the implications of various ink formulations for solution processes, elucidating inkjet printing methodologies, and exploring diverse approaches employed for both dielectric and electrode materials.

3. Ink Preparation

As described in the introduction, this review focuses on inkjet-printed IGZO, a procedure for which suitable inks must be synthesized. The following sections will discuss the working principle and the effects of the various synthesis routes for IGZO inks. The principal ink preparation techniques employed for IGZO inkjet printing encompass salt precursor ink, nanoparticle-based ink (mainly sol-gel method), electrochemical synthesis, and solution combustion synthesis.[47,64,65] Extensive research conducted in recent years has yielded diverse outcomes contingent upon the specific execution and fine-tuning of each method. The two primary challenges encountered during ink preparation relate to the ink's compatibility with inkjet printing and the subsequent performance of the fabricated devices. Concerning compatibility with inkjet printing, the ink formulation must be engineered to mitigate issues such as nozzle clogging and uneven spatial distribution.[66] Moreover, additional factors such as the coffee-ring effect, viscosity, drop formation, and spreading behavior must be meticulously addressed. Variations in ink formulations give rise to distinct behaviors in these aspects, necessitating tailored ink preparation strategies aligned with the intended application of thin films. Furthermore, the performance of thin films can vary depending on the chosen ink preparation method. Irrespective of the selected preparation technique, the presence of solvent residues in the final film is inevitable due to the respective drying behaviors of the solvents present. These residual organic components, along with remnants of ligands and ions, significantly influence film quality, morphology, and subsequent device performance, making them one of the crucial factors in every solution process technique.[47] Therefore, meticulous attention to ink formulation and processing parameters is paramount in achieving optimal performance and reproducibility in inkjet-printed thin-film devices.

3.1. Precursor-Based Inks

The preparation of inks for inkjet printing can be achieved through the use of a salt precursor-based formulation. This involves dissolving various salts in a solvent, such as deionized (DI) water or 2-methoxyethanol (2-ME), followed by agitation and aging for a specified duration. These ink formulations can be used with various solution-based techniques, including inkjet printing, spin-coating, and drop-casting. The first inkjet-printed IGZO channel layers were developed by Kim et al. in 2009.[42] In their study, they dissolved zinc acetate, gallium nitrate, and indium nitrate in 2-ME. However, the limited solubility of indium nitrate and gallium nitrate caused the IGZO ink to precipitate. To tackle this challenge, ethanolamine (EA) is an essential stabilizer when added to the ink solution. Additionally, the inclusion of acetic acid improves ink homogeneity.[42] Several researchers in the field have proposed comparable methods for synthesizing IGZO ink formulations.[40,67,68] Another approach pursued by various research groups involves simplifying the synthesis of metal oxide salt precursor-based inks by using DI water as a solvent. Although there may be slight variations in the specific parameters used in different studies, the prevailing trend is to use nitrate-based inks and stir them for two to four hours at room temperature.[69–71]

3.2. Nanoparticulate Inks

Metal oxide nanoparticles can be combined with a solvent and surfactants to create viable inks for solution processing. The solvent acts as a dispersion medium, while the surfactants prevent agglomeration of the nanoparticles, which have high surface activity and energy. An SEM image of IGZO nanoparticles can be found in **Figure 3**a. In the past, two main routes have been used to prepare IGZO nanoparticles.[72] Wu et al. developed a multistep co-precipitation method for the synthesis of IGZO nanoparticles.[73] The method involves gradually adding sodium hydroxide (NaOH) to a solution containing indium nitrate, gallium nitrate, and zinc nitrate at a temperature of 10 °C. The three phases are derived from the drastic difference in solubility product constant of the three different compounds. After filtering, washing, and drying the compound, an IGZO precursor powder remained, which was subsequently calcinated to form IGZO nanoparticles.[73] In a similar instance, Fukuda and colleagues produced IGZO nanoparticles by mixing indium nitrate, gallium nitrate, and zinc nitrate with urea, ethylene glycol (EG), and Milli-Q grade water.[74] The mixture was heated until the water evaporated and the urea decomposed, leaving behind a white precipitation that can be attributed to the metal hydroxides and carbonates. The IGZO nanoparticles were subsequently obtained by centrifuging, washing, and drying the precipitated compound.[74]

The prevalent method for nanoparticulate ink preparation in contemporary inkjet printing applications is the sol-gel technique. This process involves the conversion of a colloidal solution (referred to as sol) into a network of monomers (referred to as gel). A diagram depicting the sol-gel process can be found in Figure 3b. Sols represent a colloidal suspension of particles in a liquid. The gel constitutes the resultant macroscopic molecule, structured akin to a molecular skeleton.[75] This process, while intricate and time-consuming, yields results particularly suitable for high-end applications. Past demonstrations have shown the utilization of amorphous IGZO inks prepared via the sol-gel method, commonly employed in various solution processes.[66,76–79] In a seminal study by Choi et al., indium nitrate, gallium nitrate, and zinc acetate were dissolved in 2-ME, with the subsequent addition of EA to stabilize the solution.[76] Following stirring and heating at 70 °C for two hours, test patterns were processed via gravure printing and annealed at 550 °C, leading to ink gelling through combustion.[76] Subsequent research delved into the role of ethylene glycol in sol-gel IGZO inks. Various IGZO inks were prepared via the sol-gel

© 2024 The Author(s). Advanced Electronic Materials published by Wiley-VCH GmbH

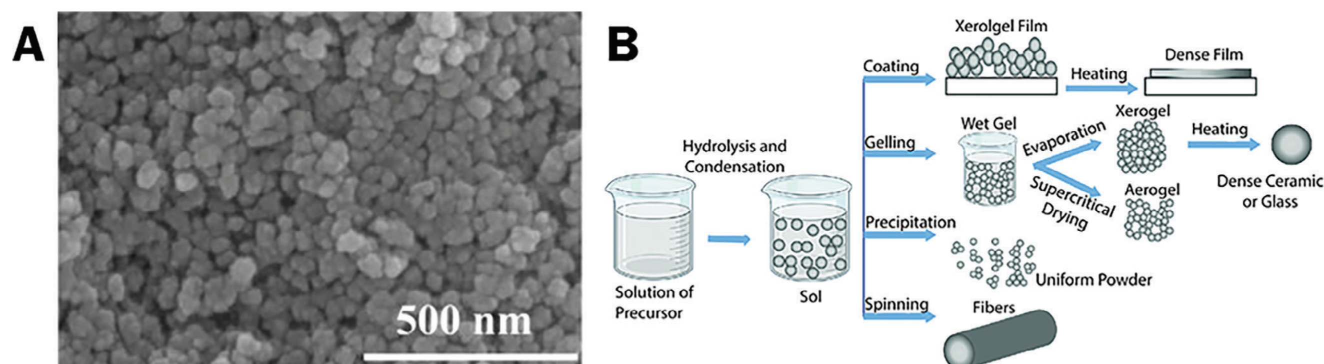

Figure 3. A) SEM image of IGZO nanoparticle. B) Diagram of the sol-gel process and the possible outcomes. (A) Reproduced with permission.[80] Copyright 2019, IEEE. (B) Reproduced with permission.[81] Copyright 2021, Jourcc.

method, utilizing similar reactants but with differing proportions of the latter.[66] EA and DI water were introduced to the solution as stabilizers. The inclusion of EG not only facilitated compatibility with inkjet printing by addressing nozzle clogging issues but also resulted in improved electrical characteristics of the printed films. EG mitigates the generation of hydroxo and oxo ligands (OH^- and O^{2-} respectively) due to chemical bonding between the deprotonated EG molecule and the metal cation. This reduction of hydroxides and oxygen vacancies in the oxide semiconductor lattice causes the aforementioned improvement of electrical characteristics.[66] Recent advancements have led to more sophisticated sol-gel formulations for IGZO inks, aiming to enhance device performance. Rajbhandari et al. dissolved indium, gallium, and zinc salts in 2-ME, followed by solvent evaporation to produce a gel, subsequently dried to obtain a powder.[79] This powder was further processed via ball milling in an acetic acid and *N*-methyl-2-pyrrolidone (NMP) mixture, then centrifuged to yield a paste. By incorporating poly-(styrene sulphonic acid) (PSSA) and poly-(vinyl alcohol) (PVA) solutions, gravure printing-ready inks were synthesized, enabling the demonstration of IGZO-based devices capable of harvesting significant portions of DC power generated by an NFC signal.[79] Another notable approach to sol-gel IGZO ink formulation for high-performance devices was introduced by Everaerts and colleagues.[78] In their combustion-based sol-gel process, indium, gallium, and zinc salts were individually dissolved in 2-ME, supplemented with aqueous ammonia and acetylacetone. Following thorough mixing and aging, the precursors were combined and utilized for inkjet printing. The resulting devices exhibited promising average (20.6 ± 4.3 cm^2 V^{-1} s^{-1}) and maximal (50 cm^2 V^{-1} s^{-1}) field-effect mobilities, underscoring the efficacy of the method.[78]

3.3. Inks Prepared by Electrochemical Synthesis

In 2015, Nadarajah et al. undertook the synthesis of an IGZO ink via electrochemical synthesis.[47] In this study, a solution containing indium nitrate, gallium nitrate, and zinc nitrate dissolved in DI water was electrolyzed. By applying a voltage between the platinum (Pt) working electrode and the Ag/AgCl reference electrode for durations ranging from 60 to 120 min, an ink-like solution was electrochemically synthesized. Following deposition, IGZO clusters ≈2 nm in size were observed, characterized by minimal counterion presence and absence of organic residues. Comparative analysis revealed that the resulting films exhibited superior structural and electrical properties when juxtaposed with reference films produced using sol-gel processed inks.[47]

3.4. Inks Prepared by Solution Combustion Synthesis

Solution combustion synthesis (SCS) is a technique derived from sol-gel and propellant chemistry that offers advantages over the sol-gel method, including faster processing, improved film quality, and lower temperature requirements.[65,82,83] SCS typically involves three key stages: the formation of a combustion mixture, gel formation, and the combustion of the gel, which triggers a self-sustained redox reaction between a fuel and an oxidant in the presence of metal cations. This reaction is initiated by an energy source, which can be thermal or electrical. The oxidants used are typically metal salts, such as metal nitrates, while the fuels are usually organic compounds rich in hydrogen and carbon, which facilitate heat generation.[65] The first reported application of SCS was published by Patil et al. in 2008.[84] Several studies have demonstrated the use of SCS in fabricating transistor devices, particularly with amorphous indium gallium zinc oxide layers, which are typically applied using techniques such as spin coating or blade coating.[65] These transistors have exhibited favorable performance metrics, including high I_{on}/I_{off} ratios of up to 10^7 and saturation mobilities of up to 20 cm^2 (Vs)$^{-1}$. In a study by Everaerts et al., inkjet-printed IGZO thin-film transistors prepared via SCS, in combination with a Hf-SAND gate dielectric, demonstrated low operating voltages (<2 V), an average field-effect mobility of 20.6 cm^2 (Vs)$^{-1}$, and an I_{on}/I_{off} ratio of 10^7.[78]

4. Inkjet Printing of IGZO TFTs

The fabrication of IGZO devices via inkjet printing requires careful consideration not only of the ink formulation but also of various auxiliary parameters, including, but not limited to, substrate, stage, and nozzle temperature, annealing techniques, and device architecture. In the subsequent sections, an overview of prior investigations into inkjet printing methodologies for IGZO will be

© 2024 The Author(s). Advanced Electronic Materials published by Wiley-VCH GmbH

2199160x, 0, Downloaded from https://onlinelibrary.wiley.com/doi/10.1002/aelm.202400478 by Karlsruher Institut F., Wiley Online Library on [10/1/2024]. See the Terms and Conditions (https://onlinelibrary.wiley.com/terms-and-conditions) on Wiley Online Library for rules of use; OA articles are governed by the applicable Creative Commons License

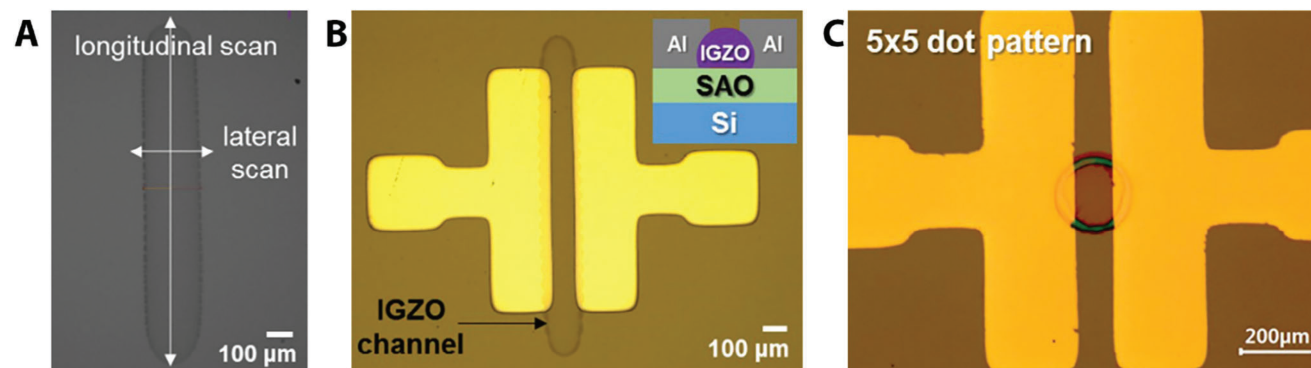

Figure 4. Optical microscope images of A) inkjet-printed IGZO stripe, B) TFT based on the in (A) shown inkjet-printed IGZO stripe with additional aluminum (Al) electrodes and Sr-doped Al_2O_3 dielectric layer, and C) TFT based on an IGZO dot with Al electrodes. (A–C) Reproduced with permission.[87] Copyright 2019, MDPI.

discussed, elucidating the multifaceted array of critical parameters essential to producing high-performance devices. To better understand the topic discussed in the following chapter, various images of IGZO TFTs prepared via inkjet printing can be found in **Figure 4**.

4.1. Temperature Requirements

A critical parameter in the inkjet printing process of IGZO is the substrate temperature. Research indicates that preheating the sample on a hotplate for a short time after printing but prior to annealing serves the dual purpose of solvent removal and positively influencing the electrical characteristics of the resultant films.[85,86] The preheating temperature is always kept lower than that of the subsequent annealing. Xie et al. conducted an extensive investigation into the impact of substrate preheating during the inkjet printing process of IGZO devices, unveiling significant enhancements in their electrical performance.[69] The study encompassed a range of preheating temperatures spanning from 40 to 275 °C, followed by annealing at 300 °C. The preheating time was set to 10 min. Notably, when subjected to a preheating temperature of 275 °C, the inkjet-printed IGZO films exhibited a remarkable tenfold increase in field-effect mobility, coupled with an I_{on}/I_{off} ratio exceeding 10^7. Moreover, the study inferred that the observed enhancement in electrical characteristics primarily stemmed from improvements in film morphology (see **Figure 5**a,b).[69] This is due to the formation of larger particle aggregations when the film is subject to higher drying temperatures, mainly due to a faster solvent evaporation process, which reflects in a reduced root-mean-square roughness of the film. Therefore, samples preheated at higher temperatures have better electrical characteristics due to an improved interface between channel and insulator due to the lower probability of discontinuity in the IGZO film.[69]

4.2. Annealing Procedures

In order to remove organic residues from solution-processed films and cause the oxidation of the nitrate salts, deposited metal oxides necessitate annealing at temperatures exceeding 400 °C at standard pressure and in most common atmospheres (O_2, N_2, air).[88] The effects of varying annealing temperatures for IGZO TFTs can be seen in Figure 5c where the transfer characteristics of devices annealed at different temperatures between 300 and 600 °C are depicted.[88] Subsequent investigations revealed that complete evaporation of organic compounds occurred

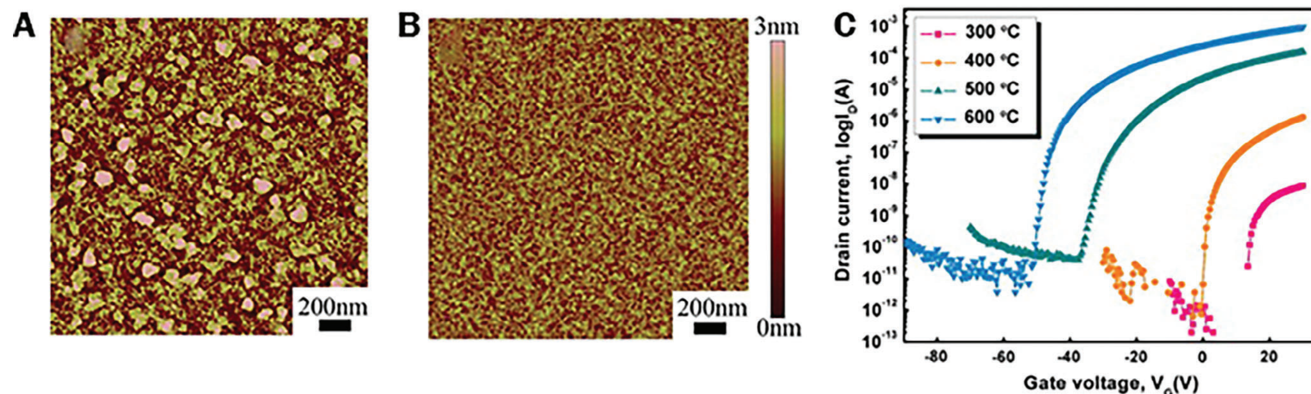

Figure 5. A) AFM image of IGZO TFTs with preheating at 40 °C and B) 275 °C before annealing at 300 °C. A) Transfer characteristics of IGZO transistors annealed at different temperatures. (A,B) Reproduced with permission.[69] Copyright 2016, The Royal Society of Chemistry. (C) Reproduced with permission.[88] Copyright 2011, Elsevier.

© 2024 The Author(s). Advanced Electronic Materials published by Wiley-VCH GmbH

2199160x, 0, Downloaded from https://onlinelibrary.wiley.com/doi/10.1002/aelm.202400478 by Karlsruher Institut F., Wiley Online Library on [10/11/2024]. See the Terms and Conditions (https://onlinelibrary.wiley.com/terms-and-conditions) on Wiley Online Library for rules of use; OA articles are governed by the applicable Creative Commons License

2199160x, 0, Downloaded from https://onlinelibrary.wiley.com/doi/10.1002/aelm.202400478 by Karlsruher Institut F., Wiley Online Library on [10/1/2024]. See the Terms and Conditions (https://onlinelibrary.wiley.com/terms-and-conditions) on Wiley Online Library for rules of use; OA articles are governed by the applicable Creative Commons License

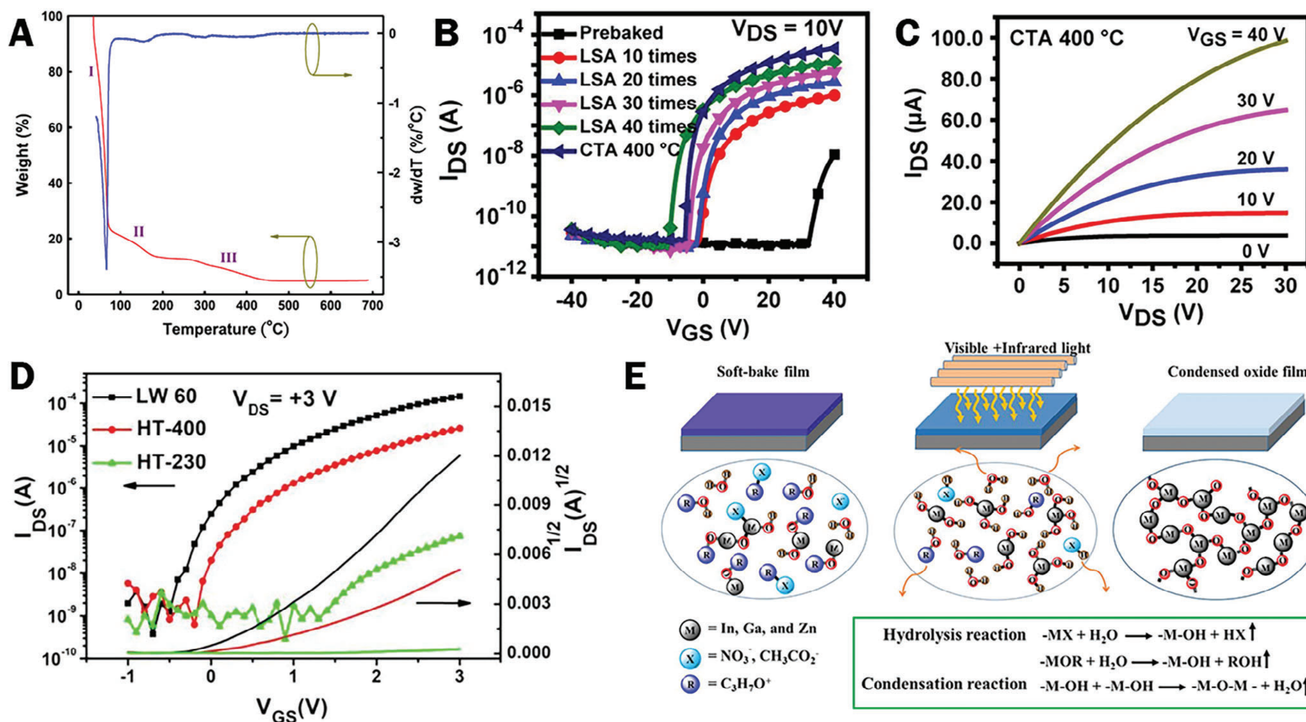

Figure 6. A) Thermogravimetric analysis of IGZO shows no more change in mass after 450 °C. B) Transfer characteristics of different IGZO TFTs subject to preheating only, laser spike annealing (LSA) treatments, and conventional thermal annealing (CTA). C) Output characteristics of IGZO TFTs after CTA at 400 °C. D) Comparison of transfer characteristics of lightwave (60 minutes, black) and conventionally (400 °C, red and 230 °C, green) annealed IGZO TFTs. E) Schematic of the condensation mechanism by lightwave annealing. (A) Reproduced with permission.[90] Copyright 2013, Elsevier. (B,C) Reproduced with permission.[100] Copyright 2017, Springer. (D,E) Reproduced with permission.[108] Copyright 2021, Elsevier.

at 450 °C (see **Figure 6a**), a temperature at which the films exhibited decreased resistivity compared to annealing at 500 °C. This is due to the decrease in carrier concentration with an increase in temperature paired with the relatively constant mobility (in the range of 400–600 °C), effectively increasing the sheet resistance with an increase in annealing temperature.[89] Consequently, this established 450 °C as the optimal annealing temperature for amorphous IGZO films.[90] For the formation of a crystalline phase in IGZO, which allows for higher ambient stability due to an increase in anticorrosive properties, annealing temperatures of 600–700 °C are required.[79,91] However, these elevated temperatures are not compatible with all types of substrates, particularly flexible organic substrates which cannot withstand such thermal stress.[66] Hence, there arises a pressing need to explore alternative annealing methodologies. In recent years, a plethora of innovative techniques have emerged to address this challenge. These include O_2/O_3 annealing,[92] microwave annealing,[93,94] ultraviolet-assisted annealing,[95] self-combustion reaction,[83] high-pressure annealing,[96] lightwave-derived annealing,[97] precursor engineering,[98] dual active layer approaches,[99] and laser spike annealing.[100] Each of these methodologies aims to mitigate substrate heating while fulfilling the requirements for film activation and oxidation, thereby expanding the applicability of IGZO deposition processes to a wider range of substrate materials and configurations.

Within the domain of high thermal budget annealing methodologies, Kim et al. proposed a two-step thermal annealing technique involving sequential stages of rapid thermal annealing (RTA) at 600 °C followed by conventional thermal annealing (CTA) at 500 °C.[101] The RTA phase yielded heightened on-current characteristics; however, concomitantly escalated off-current was observed. The rapid heating and cooling processes in RTA cause an increase in interface traps, which are responsible for the aforementioned high off-current. This adverse effect was subsequently alleviated by the ensuing CTA process, resulting in a reduction of off-current levels.[101]

Laser spike annealing (LSA) has been demonstrated to be a viable alternative to conventional thermal annealing for high-performance IGZO TFTs while reaching maximal temperatures of 200 °C only during the prebaking process (see Figure 6b,c).[100] LSA involves rapidly elevating the temperature of the film for a brief duration, facilitated by a scanning laser source while minimizing the risk of thermal damage to the substrate.[102–104]

Another promising annealing technique for IGZO TFTs is high-pressure annealing. In this method, solution-processed IGZO devices undergo a sequential annealing process comprising prebaking at 300 °C, thermal annealing under vacuum at 300 °C, and extended thermal annealing at 350 °C under various ambient gases (N_2, O_2, and air). During the final phase, the pressure was systematically adjusted, ranging from ambient pressure to 4 MPa, to assess the optimal pressure settings.

Significantly improved electrical characteristics have been observed (field effect mobility and subthreshold swing improvements) compared to devices subjected to conventional thermal annealing at equivalent temperatures, with optimal performance achieved under high-pressure annealing conditions of 1 MPa in

© 2024 The Author(s). Advanced Electronic Materials published by Wiley-VCH GmbH

an O_2 atmosphere.[105] This is probably due to the densification of the film, causing the particles to move closer together as well as to the decrease in defects inside the bulk IGZO material and at the interfaces. When the pressure is increased further, over-oxidation due to the diffusion of O_2 into the material causes a deterioration of electrical properties.

By making use of the molecular vibrational spectrum in the infrared region,[106] an annealing procedure for IGZO has been presented, where infrared light is used. This method maintains a strict temperature limit of 300 °C during the annealing process and exhibits favorable electrical properties suitable for TFT device functionality.[107] Additionally, harnessing the infrared segment of the light spectrum, lightwave-induced annealing has been employed to fabricate high-quality IGZO films suitable for TFT applications (see Figure 6d). This method involves the utilization of a halogen lamp to irradiate the sample with light spanning from ultraviolet to infrared wavelengths, effectuating annealing through light-induced heat. Figure 6e depicts a schematic diagram of the lightwave annealing process. Throughout the entire process, temperatures are rigorously maintained below 230 °C.[97] Recent advancements have showcased IGZO TFTs with mobilities reaching up to 13.4 $cm^2 V^{-1} s^{-1}$, surpassing those of reference samples annealed via conventional thermal methods at 230 °C. Thus, this technique emerges as a viable annealing strategy for applications where elevated temperatures could potentially compromise substrate integrity.[108]

Microwave annealing presents a compelling alternative to traditional thermal annealing methods owing to its heightened thermal efficiency and reduced thermal budget, while typically lasting only a few minutes. This technique leverages microwave energy to rapidly heat the target layers, expediting oxidation processes compared to conventional thermal annealing approaches. The microwave power and frequency must be compatible with the chosen substrate and other previously deposited materials to avoid overheating and other heat-related damages. Experimental investigations conducted on IGZO have revealed notable enhancements in electrical characteristics of the films, boasting improved field effect mobility, threshold voltage, I_{on}/I_{off} ratio, subthreshold swing, and interface trap density, translating into improved performance of TFT devices when compared to conventionally annealed counterparts.[109] Furthermore, comparative studies have demonstrated that IGZO TFTs subjected to microwave annealing exhibit electrical properties akin to those of devices annealed thermally for an extended duration of two hours.[110] Noteworthy within this realm of research is the discernible disparity in annealing duration between microwave annealing and conventional thermal annealing methodologies.[111]

To optimize microwave annealing further, it can be integrated with a subsequent conventional thermal post-annealing step, which has been shown to further enhance device characteristics albeit at the expense of compatibility with flexible substrates due to the required high thermal budget.[112,113] To circumvent this limitation, microwave annealing can be synergistically combined with vacuum ultraviolet (VUV) irradiation. Cheong et al. demonstrated that this combined approach not only improved the electrical properties of IGZO TFTs compared to thermally annealed reference devices but also significantly reduced the duration of the post-annealing process from over one hour to merely one minute.[111] This exemplifies how alternative annealing techniques can broaden the spectrum of compatible substrate materials while concurrently enhancing production throughput through reduced annealing times.

A summary table of the annealing techniques with the corresponding electrical characteristics for each referenced sample can be found in **Table 1**.

4.3. Inkjet Printing Challenges

Numerous factors exert influence on the quality of printed films and devices in the inkjet printing of metal oxides. Among the most prominent are ink viscosity, which dictates the distribution and morphology of the dried film owing to phenomena such as the coffee-ring effect, and film thickness, a critical determinant for achieving high-performance devices. Optimizing these parameters leads to crack-less films and, as a result thereof, to high-performance devices. Upon drying of a metal oxide ink on a surface, rapid evaporation of the outer solvent layer leads to the accumulation of material at the periphery, forming what is commonly referred to as the three-phase contact line, where liquid, gas, and solid phases converge (see **Figure 7a,b**).[114,115] This phenomenon, known as the coffee-ring effect, poses significant challenges to both film quality and resultant device performance. Firstly, the non-uniform thickness gradient across the film can impede device functionality by inducing undesirable series resistance due to inadequate electrode-channel layer contact. Secondly, the formation of a shallow, thinner region at the film center may hinder carrier transport.[42] One strategy to mitigate the coffee-ring effect involves controlling material flow on the substrate or manipulating the movement of the three-phase contact line.[116] However, a common issue encountered with such mitigation techniques pertains to the resultant film morphology, often characterized by a dome-like structure with thicker central regions tapering toward the periphery.[117] Effects of surface treatment with hexamethyldisilazane (HMDS) can be seen in Figure 7d,e. Concurrently, investigations into ink composition have highlighted the efficacy of blending solvents with varying boiling points to mitigate the coffee-ring effect, leveraging differences in surface tension between the constituent solvents.[118] Additionally, studies have underscored the significant impact of metal precursor concentration, and consequently ink viscosity, on the quality of inkjet-printed droplets. The increase in viscosity causes the solution to diffuse slower on the substrate, thereby enhancing film uniformity and ameliorating the coffee-ring effect.[100] The viscosity of inks suitable for inkjet printing is a critical parameter, influencing not only the coffee-ring effect but also the overall printability of the ink. Contemporary inkjet printers equipped with piezoelectric print heads typically accommodate inks with viscosities in the range of 8–15 cP, whereas thermal print heads are limited to inks with viscosities of up to 3 cP.[119] Moreover, viscosity exhibits temperature dependence, resulting in variations between ambient conditions and the elevated temperatures encountered during printing. Consequently, a current objective in inkjet printing technology is the development of inks with temperature-independent viscosities, spanning from room temperature (e.g., in the cartridge) to printing conditions (e.g., in the nozzle).[119]

© 2024 The Author(s). Advanced Electronic Materials published by Wiley-VCH GmbH

2199160x, 0, Downloaded from https://onlinelibrary.wiley.com/doi/10.1002/aelm.202400478 by Karlsruher Institut F., Wiley Online Library on [10/11/2024]. See the Terms and Conditions (https://onlinelibrary.wiley.com/terms-and-conditions) on Wiley Online Library for rules of use; OA articles are governed by the applicable Creative Commons License

Table 1. Summary of annealing techniques referenced in this paper with corresponding sample data. RTA: rapid thermal annealing. CTA: conventional thermal annealing. Post RTA: 30 min. CTA process after RTA. HPA: high-pressure annealing. IRA: infrared annealing. UV/ozone: 150 min. UV/ozone treatment before CTA. MWA: microwave annealing. VUV: vacuum ultraviolet light treatment. LSA: laser-spike annealing. A visual representation of the mobilities and I_{on}/I_{off} ratios presented in this table can be found in Figure 7c.

#	Deposition method	Annealing method	Max. annealing temp. [°C]	Mobility [cm^2 V^{-1} s^{-1}]	I_{on}/I_{off}	Year	Source
1	Spin-coating	RTA	400	3,40E-02	1,00E+03	2010	[89]
2	Spin-coating	RTA	600	1,3E+00	2,50E+04	2010	[89]
3	Spin-coating	RTA	800	1,70E-03	3,10E+04	2010	[89]
4	Spin-coating	HPA O_2 1MPa	300	1,02E+00	7,50E+06	2011	[105]
5	Spin-coating	HPA O_2 1MPa	350	3,30E+00	5,40E+06	2011	[105]
6	Spin-coating	HPA N_2 1MPa	350	2,78E+00	8,60E+06	2011	[105]
7	Spin-coating	HPA Air 1MPa	350	1,34E+00	2,00E+06	2011	[105]
8	Spin-coating	RTA	600	7,80E-01	1,05E+05	2013	[101]
9	Spin-coating	CTA	600	7,80E-03	2,05E+05	2013	[101]
10	Spin-coating	RTA + post RTA @ 300 °C	600	3,20E-01	6,75E+06	2013	[101]
11	Spin-coating	RTA + post RTA @ 400 °C	600	4,70E-01	4,73E+06	2013	[101]
12	Spin-coating	RTA + post RTA @500 °C	600	7,80E-01	5,34E+06	2013	[101]
13	Spin-coating	IRA @1,72 W cm^{-2} for 60 min.	240	2,70E-02	3,52E+03	2013	[107]
14	Spin-coating	IRA @1,89 W cm^{-2} for 60 min.	260	1,70E-01	5,54E+03	2013	[107]
15	Spin-coating	IRA @2,16 W cm^{-2} for 60 min.	280	4,70E-01	6,03E+04	2013	[107]
16	Spin-coating	IRA @2,54 W cm^{-2} for 60 min.	300	1,08E+00	3,04E+05	2013	[107]
17	Spin-coating	UV/ozone 60 min. + CTA	300	4,40E-01	1,40E+05	2013	[112]
18	Spin-coating	UV/ozone 120 min. + CTA	300	2,45E-01	1,10E+06	2013	[112]
19	Spin-coating	UV/ozone 180 min. + CTA	300	5,60E-01	1,30E+06	2013	[112]
20	Spin-coating	MWA for 5 min.	200	1,40E-04	1,00E+04	2015	[111]
21	Spin-coating	MWA for 5 min. + VUV	200	3,00E-01	1,00E+08	2015	[111]
22	Inkjet printing	CTA	400	1,60E+00	2,16E+06	2017	[100]
23	Inkjet printing	LSA 10 times	200	7,00E-02	1,01E+05	2017	[100]
24	Inkjet printing	LSA 40 times	200	1,50E+00	1,29E+06	2017	[100]
25	Spin-coating	IRA for 15 min.	230	1,07E+01	1,00E+05	2018	[97]
26	Spin-coating	IRA for 60 min.	230	6,13E+01	1,00E+06	2018	[97]
27	Spin-coating	IRA for 90 min.	230	6,82E+01	1,00E+04	2018	[97]
28	Spin-coating	MWA @250 W for 2 min.	540	7,50E-01	1,87E+06	2019	[109]
29	Spin-coating	MWA @750 W for 2 min.	540	9,20E-01	2,02E+06	2019	[109]
30	Spin-coating	MWA @1400 W for 2 min.	540	1,13E+00	2,90E+06	2019	[109]
31	Spin-coating	MWA @1800 W for 2:30 min.	540	1,16E+00	2,98E+06	2019	[109]
32	Spin-coating	MWA @1800 W for 3:30 min.	540	5,41E+00	1,57E+07	2019	[109]
33	Spin-coating	MWA @1800 W for 4:30 min.	540	6,43E+00	1,40E+07	2019	[109]

Another crucial aspect in the formulation of inkjet-compatible inks is the shear forces generated within the printhead nozzles during operation. Newtonian fluids, which maintain a constant viscosity across a wide range of shear forces, remain the preferred standard for inkjet printing applications.[119]

Minimizing the size and interdot distance of inkjet-printed metal oxide droplets, often called feature size, holds paramount significance, particularly for active-matrix organic light-emitting diode (AMOLED) driving TFTs, which necessitate continual size reduction to accommodate higher pixel densities. The droplet diameter is contingent upon factors including the aforementioned three-phase contact line, substrate surface properties, and ink viscosity.[116,120] To achieve small dots, which are generally preferred for micro- and nanoelectronics applications, the rule of thumb states that the inks should have a higher surface tension compared to that of the substrate.[121,122] To diminish the minimum spacing between inkjet-printed IGZO dots, Wu et al. pursued a dual-pronged strategy involving hydrophobic treatment of the substrate surface and polyvinylpyrrolidone (PVP) doping of the IGZO ink.[71] Reduction in droplet size correlates with an augmented contact angle between the droplet and substrate, achievable using water as a solvent, known for its inherently high contact angle, and substrate treatment with HMDS or OTS self-assembly to impart hydrophobicity to the substrate. However, alongside the diminution in droplet size, IGZO film thickness tends to increase. To mitigate this phenomenon, PVP is incorporated to delay droplet shrinkage, a method found effective, particularly on HMDS-treated substrates.[71] Inks with higher viscosity exhibit slower flow behavior on the substrate compared to low-viscosity inks. This characteristic can be exploited to further

 © 2024 The Author(s). Advanced Electronic Materials published by Wiley-VCH GmbH

2199160x, 0, Downloaded from https://onlinelibrary.wiley.com/doi/10.1002/aelm.202400478 by Karlsruher Institut F., Wiley Online Library on [10/11/2024]. See the Terms and Conditions (https://onlinelibrary.wiley.com/terms-and-conditions) on Wiley Online Library for rules of use; OA articles are governed by the applicable Creative Commons License

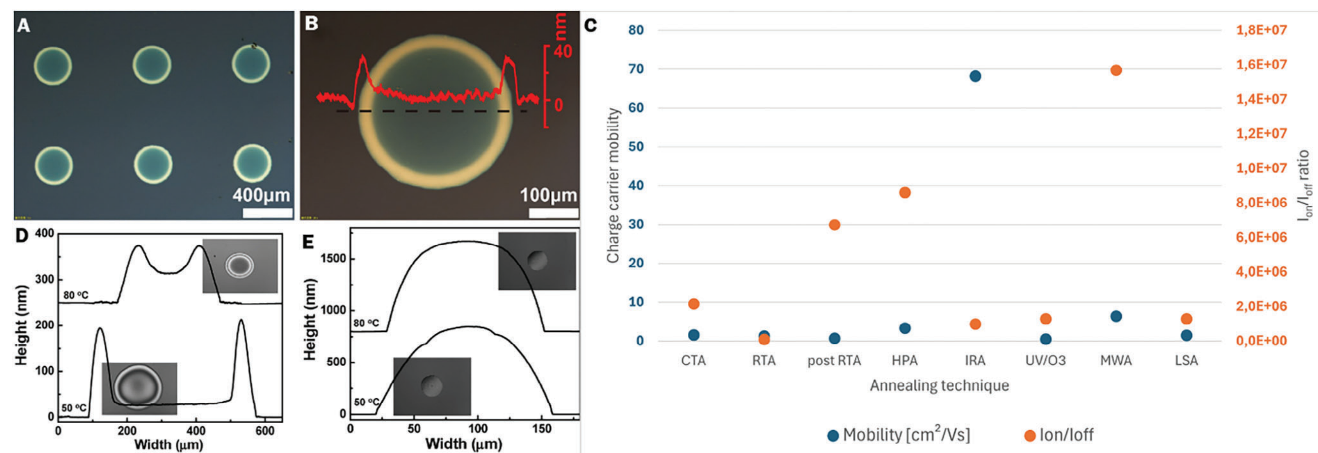

Figure 7. A,B) Optical microscope images and height profile of inkjet-printed IGZO drops that show clear coffee-ring artefacts. C) Graph depicting the highest achieved mobility and I_{on}/I_{off} ratio with IGZO transistors annealed with various annealing techniques. All data is reported precisely in Table 1. D) Height profiles of inkjet-printed ZTO dots on IPA-cleaned and E) HMDS-treated SiO_2 substrate. (A,B) Reproduced with permission.[100] Copyright 2017, Springer. (D,E) Reproduced with permission.[117] Copyright 2009, American Chemical Society.

reduce feature size during printing. The spreading of ink droplets can be modulated through the incorporation of volatile solvents, which evaporate rapidly, leading to a prompt increase in viscosity as solvent evaporation progresses.[119] The lateral resolution of printed structures is, in parts, influenced by the droplet volume, which in parts also influences the film thickness. As mentioned earlier, the concomitant increase in film thickness poses challenges to the properties of fabricated IGZO TFTs as well,[58,123,124] suggesting that an optimal film thickness exists. This optimal film thickness was determined in a study by Wang et al., where inkjet-printed IGZO TFTs were fabricated with varying channel layer thicknesses ranging from 23 to 125 nm. Their analysis determined the optimal channel thickness to be 55 nm.[49]

The formation of bubbles and foam within printed layers represents another significant factor that can introduce defects, ultimately diminishing the performance of the device. This phenomenon frequently arises from the inclusion of surfactants in the ink, which are commonly employed to regulate the surface tension of the printed droplets.[119] During the evaporation of the solvent, foam or bubbles may create voids within the material, resulting in a compromised structure with inferior properties. To mitigate this issue, defoamers are often incorporated to promote the breakdown of unwanted foam. However, it is important to note that the use of defoamers significantly reduces the shelf life of the ink, as these agents tend to separate from the solution over time.[119]

A significant challenge in inkjet printing is nozzle clogging, which can result from several factors. One common cause is the presence of aggregates or impurities within the ink that exceed the nozzle diameter.[125] Additionally, gelation of the ink due to high shear forces[126–128] and hydrodynamic bridging[129]—a process in which multiple particles simultaneously reach the nozzle and form a bridge—can obstruct the nozzle even when the individual particles are smaller than the nozzle opening. Beyond these aggregation-related mechanisms, nozzle clogging can also arise from unintended drying.[125] This phenomenon, often referred to as fouling, encompasses several processes at the nozzle, such as the drying of surfactants within the ink or the crystallization of solvent components.[130] Environmental contaminants, including dust or debris within the cartridge or reaction byproducts generated during ink heating, can further contribute to nozzle blockages, leading to inconsistent droplet ejection or complete nozzle failure.[131]

4.4. Figures of Merit

To facilitate a more precise comparison of the various devices reported in the literature, it is essential to introduce and consistently report key performance metrics, also referred to as figures of merit. For transistors, these critical parameters typically include mobility, which can be categorized into saturation, field-effect, and Hall mobility; threshold voltage, which denotes the voltage at which the transistor transitions to the on-state; the I_{on}/I_{off} ratio, representing the ratio between the leakage current (off-state) and the operational current (on-state); and the subthreshold swing (SS). In the context of inkjet-printed transistors, additional metrics such as feature size, which describes the minimum achievable length and width of the device, and the final thickness of the various layers are particularly significant.

As discussed earlier in this review, most devices reported in the literature are fabricated using spin-coating, a well-established technique with fewer limitations compared to inkjet printing, especially in laboratory-scale applications. Consequently, the number of inkjet-printed IGZO-based transistors reported in the literature has been relatively limited. Among the existing reports, these transistors exhibit saturation mobilities ranging from 0.012 to 6.42 $cm^2\ (Vs)^{-1}$, threshold voltages between −33.8 and 25.6 V, and I_{on}/I_{off} ratios from 10^3 to 10^7. A comprehensive list of inkjet-printed IGZO transistors published in the past eight years, along with their corresponding figures of merit, is provided in **Table 2**.

4.5. Device Architecture

Limited investigation has been conducted regarding the device architecture of inkjet-printed IGZO TFTs, yet the findings have

© 2024 The Author(s). Advanced Electronic Materials published by Wiley-VCH GmbH

2199160x, 0, Downloaded from https://onlinelibrary.wiley.com/doi/10.1002/aelm.202400478 by Karlsruher Institut F., Wiley Online Library on [10/1/2024]. See the Terms and Conditions (https://onlinelibrary.wiley.com/terms-and-conditions) on Wiley Online Library for rules of use; OA articles are governed by the applicable Creative Commons License

Table 2. Recently published inkjet-printed IGZO transistors arranged by date of publication. S.S.: subthreshold swing. V_{th}: threshold voltage.

Thickness	μ_{SAT} [cm^2 (Vs)$^{-1}$]	V_{th} [V]	I_{on}/I_{off}	S.S. [V dec^{-1}]	DE/C	Source
–	0.31	11	10^6	1.18	SiO_2/Al	[69]
–	0.56	14	10^6	1.53	SiO_2/Al	[69]
–	1.05	18	10^7	2.04	SiO_2/Al	[69]
–	4.93	8	10^7	0.93	SiO_2/Al	[69]
15 nm	2.16	25.6	10^5	4.87	SiO_2/Graphene	[77]
15 nm	3.31	22.2	10^5	5.12	SiO_2/Graphene	[77]
15 nm	4.32	16.1	10^5	2.49	SiO_2/Graphene	[77]
15 nm	5.42	18.4	10^5	2.74	SiO_2/Graphene	[77]
15 nm	6.38	7.2	10^5	4.28	SiO_2/Graphene	[77]
15 nm	6.42	7.9	10^5	4.57	SiO_2/Graphene	[77]
–	0.07	0	10^5	3.43	SiO_2/Au	[100]
–	0.20	−2	10^5	2.09	SiO_2/Au	[100]
–	0.61	−5	10^5	1.91	SiO_2/Au	[100]
–	1.50	−8.5	10^6	1.66	SiO_2/Au	[100]
–	1.60	−5	10^6	0.94	SiO_2/Au	[100]
30 nm	0.323	12.3	10^4	–	SiO_2/Ag	[132]
120 nm	0.012	11.2	10^3	–	SiO_2/Ag	[132]
–	0.23	−27.8	10^7	–	SiO_2/Al	[87]
–	0.37	−33.8	10^7	–	SiO_2/Al	[87]
50–70 nm	2.2 (μ_{Hall})	4–6	–	–	NH4OH:H2O2:H2O/Ag	[68]

been substantive. In one study, wherein bottom-gate top-contact and bottom-gate bottom-contact devices were fabricated, it was observed that bottom-contact devices exhibited nearly double the mobility compared to top-contact devices, albeit with higher threshold voltage.[40] Subsequent investigations explored the performance of top-contact, bottom-contact, and middle-contact device architectures with inkjet-printed IGZO TFTs. The results unveiled that top-contact devices displayed heightened nonlinearity in output curves at low source-drain voltages but exhibited higher saturation current compared to bottom-contact devices. This disparity was ascribed to the rough surface upon which bottom-contact devices were printed. Particularly noteworthy was the introduction of the novel middle-contact approach, which not only manifested linear output curves at low source-drain voltages but also achieved saturation currents surpassing both top-contact and bottom-contact devices. The superior performance of this architectural approach is likely attributable to the high-quality film printed before contact formation, coupled with the favorable characteristics of the electrode/IGZO interface observed in bottom-contact devices.[77]

4.6. Bilayer Configurations

In the past decade, considerable attention has been directed towards bilayer IGZO structures as potential enhancers of device characteristics, particularly through the incorporation of a higher conductivity layer as the second channel. Rim et al. elucidated the efficacy of this approach by demonstrating notable improvements in IGZO-based TFTs through the utilization of indium-tin-zinc oxide (ITZO) layers as the top-channel material in a bilayer configuration (see **Figure** 8a,b). Their experimental findings revealed a significant fifteenfold increase in saturation mobility for the bilayer devices compared to their single-layer IGZO counterparts.[133] Subsequent investigations by Nadarajah et al. expanded upon these findings, wherein IGZO inks were prepared via electrochemical synthesis, resulting in even more promising outcomes. The ITZO/IGZO bilayers exhibited saturation mobility (μ_{SAT}) of 30 cm^2 V^{-1} s^{-1}, a notable enhancement over the 22 cm^2 V^{-1} s^{-1} reported in the prior study.[47,133]

In a parallel endeavor, Liang et al. pursued an alternative approach to solution-processed IGZO bilayer structures by incorporating indium oxide (In_2O_3).[70] Through meticulous tuning of inkjet printing parameters and UV/ozone treatment, they discerned that the morphology of the indium oxide layer correlates with the concentration of the metal precursor in the ink. Moreover, they noted that insufficient spacing between IGZO droplets could lead to ink overflow and consequent deterioration of device characteristics.[70] A schematic depicting the printing process of the devices can be found in Figure 8c. Leveraging these insights into the interplay between morphology and electrical properties, high-performance In_2O_3/IGZO bilayer devices boasting a mobility of 14.5 cm^2 V^{-1} s^{-1} were successfully realized (see Figure 8d).[70] Similarly, Shao et al. achieved even higher mobility values (18.78 cm^2 V^{-1} s^{-1}) through meticulous parameter optimization, although they caution that a delicate balance between UV/ozone treatment and O_2-plasma cleaning is necessary to maximize device performance.[134] Prolonged O_2-plasma cleaning was found to further enhance mobility but also led to a shift in the threshold voltage, posing challenges in the operation of the devices as thin-film transistors.[134] Notably, Shao et al. also introduced the first In_2O_3/IGZO bilayer NMOS inverter

© 2024 The Author(s). Advanced Electronic Materials published by Wiley-VCH GmbH

2199160x, 0, Downloaded from https://onlinelibrary.wiley.com/doi/10.1002/aelm.202400478 by Karlsruher Institut F., Wiley Online Library on [10/11/2024]. See the Terms and Conditions (https://onlinelibrary.wiley.com/terms-and-conditions) on Wiley Online Library for rules of use; OA articles are governed by the applicable Creative Commons License

2199160x, 0, Downloaded from https://onlinelibrary.wiley.com/doi/10.1002/aelm.202400478 by Karlsruher Institut F., Wiley Online Library on [10/1/2024]. See the Terms and Conditions (https://onlinelibrary.wiley.com/terms-and-conditions) on Wiley Online Library for rules of use; OA articles are governed by the applicable Creative Commons License

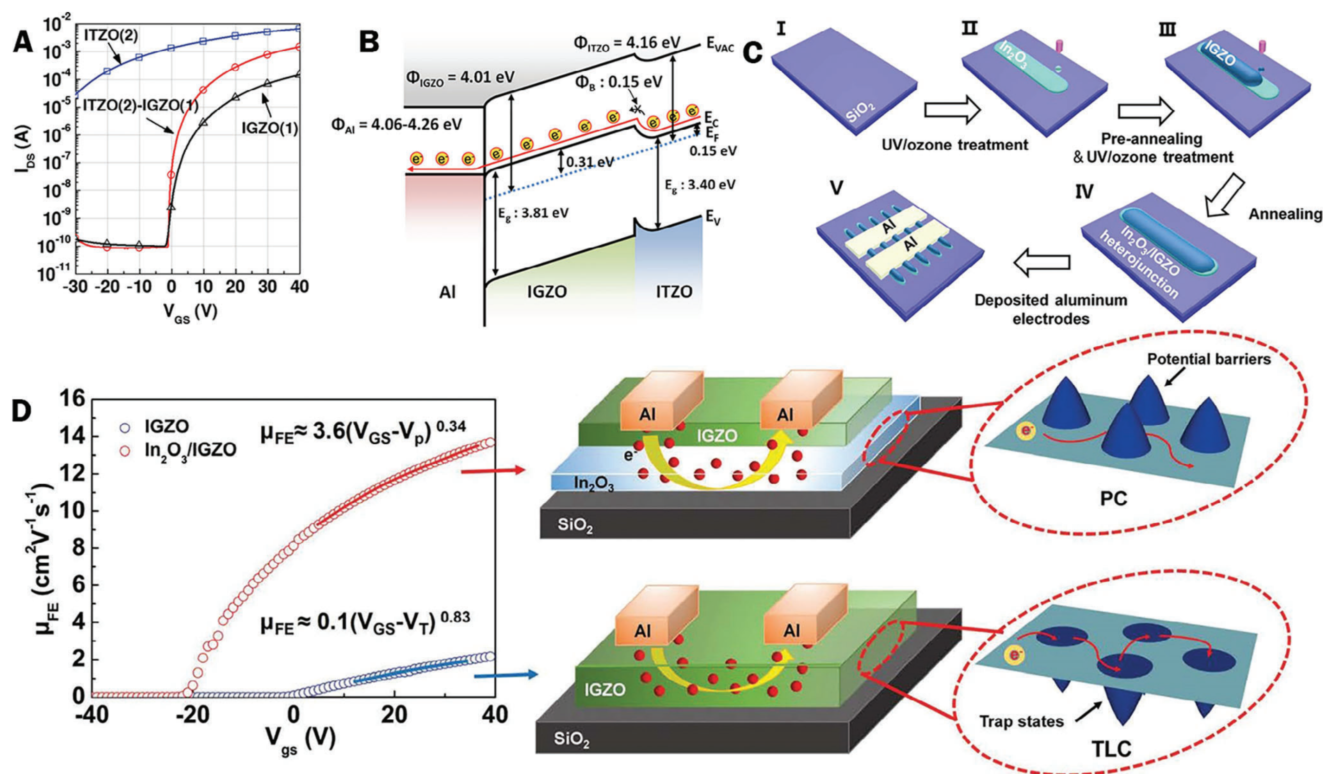

Figure 8. A) Transfer characteristics of ITZO, IGZO, and ITZO/IGZO bilayer TFTs. B) Band diagram of ITZO/IGZO heterojunction with aluminum (Al) contacts. C) Schematic depicting the process of inkjet-printing In_2O_3/IGZO bilayer line structures and subsequent contacting. D) Relation between field effect mobility and gate voltage of In_2O_3/IGZO bilayer TFTs (red) and single layer IGZO TFTs (blue) accompanied by a visualization of the respective transmission paths of electrons. (A,B) Reproduced with permission.[133] Copyright 2014, Wiley. (C,D) Reproduced with permission.[70] Copyright 2019, The Royal Society of Chemistry.

during their investigation, suggesting unexplored avenues for future applications.[134]

It is pertinent to mention the comparative evaluation conducted by Tiwari et al., wherein sputtered IZO/ZnO/IGZO trilayers were compared to sputtered IZO/IGZO bilayers.[135] The researchers observed that the ultrathin 2 nm ZnO layer effectively mitigates both oxygen and zinc vacancies in the IZO top layer, resulting in superior electrical characteristics compared to the bilayer configuration. While the fabrication of stacked microstructures via inkjet printing poses current challenges, ongoing research in this direction holds promise for realizing devices with even greater performance metrics.[135]

4.7. Dielectrics

For a long time, SiO_2 has conventionally served as the predominant dielectric material for transistors, owing to its facile fabrication process on silicon substrates. However, high-κ materials have emerged as superior alternatives for gate dielectrics.[136] Among the notable oxides employed for IGZO dielectrics are aluminum oxide (Al_2O_3) and zirconium oxide (ZrO_2).[68,137] Certain challenges associated with inkjet printing, which are also evident when printing a TFT channel, mainly manifest during the printing of dielectric layers. Inkjet printing typically produces rougher films in comparison to techniques such as spin coating or sputtering. Additionally, as with many solution-based processes, the unpredictable drying dynamics of the solvent often lead to non-uniform layer formation.[138] These defects present significant obstacles when attempting to print a second layer atop a previously printed one. Achieving thin, pinhole-free semiconducting channels and dielectric layers remains a persistent challenge.[138] Previous studies have demonstrated the successful inkjet printing of AlO_x and ZrO_2, though the printing of other binary and ternary oxide dielectrics is still in its early stages of research.[139–143] A cost-effective ink formulation for Al_2O_3 has been successfully devised, facilitating the fabrication of IGZO TFTs with inkjet-printed dielectrics exhibiting commendable performance characteristics.

Furthermore, investigations into inkjet-printed ZrO_2 dielectrics for IGZO TFTs analyzed through a multilayer approach, wherein multiple layers of ZrO_2 are deposited atop one another, yielded that the bilayer configuration demonstrated the lowest leakage current density.[137] While binary metal oxides offer higher dielectric constants, the associated bandgap tends to diminish with increasing dielectric constant.[144] To address this issue, recent research efforts have focused on the integration of wide bandgap oxides with high-κ oxides, leading to the development of dielectric materials that exhibit dielectric constants higher than the lower-κ oxide while maintaining a bandgap comparable to that of the wide bandgap oxide.[139] Solution-based methods, such as spin coating and spray pyrolysis, have

 © 2024 The Author(s). Advanced Electronic Materials published by Wiley-VCH GmbH

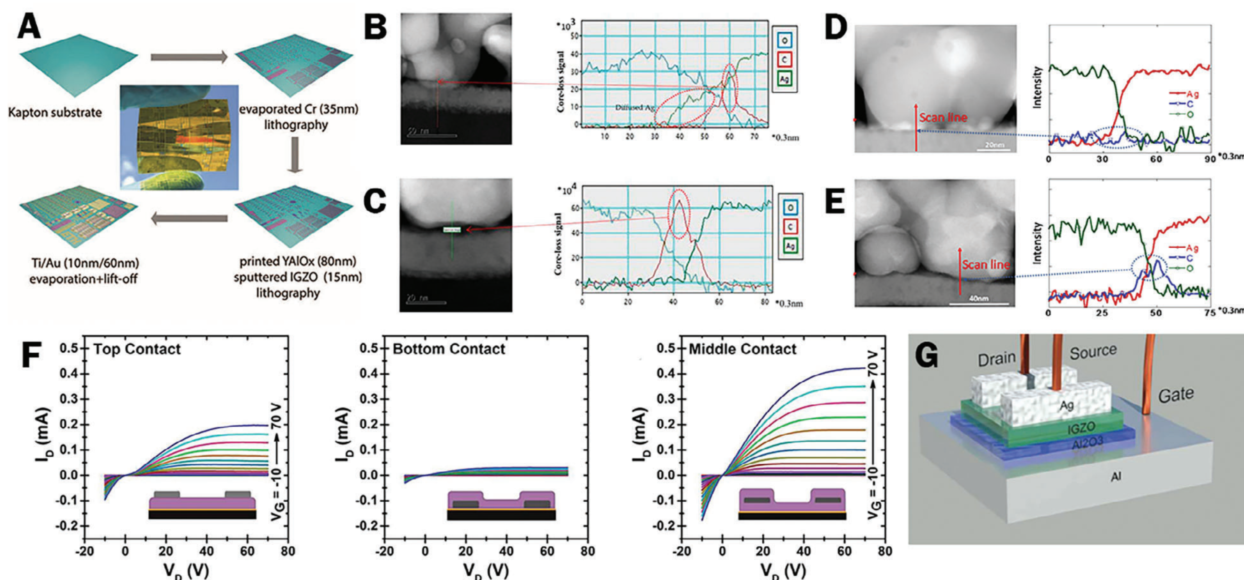

Figure 9. A) Schematic diagram of the fabrication process of IGZO TFTs with $YAlO_x$ dielectric layer on a flexible substrate. B) EELS analysis of the interface between silver electrodes and IGZO shows a lower amount of carbon at the interface when the substrate is heated to 60 °C when printing compared to C) printing at room temperature as well as when D) salt precursor-based inks are used compared to E) nanoparticle-based ink. F) Output characteristics of IGZO TFTs with graphene electrodes for various device architectures demonstrate that the novel middle contact architecture boasts the best characteristics. G) Schematic of first fully printed IGZO device by Arjmandi et al. (A) Reproduced with permission.[152] Copyright 2019, Wiley. (B,C) Reproduced with permission.[174] Copyright 2017, MDPI. (D,E) Reproduced with permission.[173] Copyright 2017, MDPI. (F) Reproduced with permission.[77] Copyright 2016, American Chemical Society. (G) Reproduced with permission.[68] Copyright 2021, IEEE.

been extensively utilized to fabricate various ternary metal oxide dielectrics. Examples of these materials include $ZrAlO_x$,[145] $HfLaO_x$,[146] $AlPO$,[147] $SrTa_2O_6$,[148] $LaAlO_3$,[149,150] $MgTiO$,[151] and $Y_xAl_{2-x}O_3$.[152–154] The latter was used by Bolat et al. in their investigation of ternary metal oxides, with the goal of synthesizing high-performance dielectrics.[152] Moreover, they explored the performance of $YAlO_x$ annealed via deep ultraviolet (DUV) annealing, successfully demonstrating high-performance dielectrics fabricated at temperatures as low as 150 °C, rendering them compatible with flexible substrates.[152] **Figure 9**a depicts a schematic of the process. DUV annealing has also shown efficacy with binary metal oxides in previous studies.[140] Carlos et al. proposed an alternative strategy involving the combination of various binary metal oxide dielectrics to further enhance transistor performance.[155] Their method employed the preparation of multilayer dielectrics via solution combustion synthesis, followed by deep-UV annealing. All devices utilized IGZO channels and thermally evaporated aluminum electrodes, while the dielectric layers were varied among mono-, bi-, and trilayer structures composed of AlO_x, HfO_x, or combinations thereof. The dielectric layers were annealed via low-temperature deep-UV annealing, which could leave organic residue or defects in the gate dielectric and therefore explain the observed hysteresis in the transfer curve. Their results indicated that the highest I_{on}/I_{off} ratio was achieved with a bilayer HfO_x/HfO_x dielectric. Additionally, the highest saturation mobilities were observed for the HfO_x/HfO_x bilayer, the $HfO_x/AlO_x/HfO_x$ trilayer, and the AlO_x/HfO_x bilayer, in that order.[155] It is worth noting that cellulose, the most abundant biopolymer in nature, presents itself as a viable alternative for gate dielectrics, characterized by biodegradability, high transparency, low leakage current, and high effective capacitance.[156] Several devices featuring cellulose dielectric layers have been previously demonstrated,[157–162] with Zhou et al. developing a cellulose nanofibril ink suitable for inkjet printing and compatible with IGZO channels, yielding results comparable to those obtained with other commonly utilized solution-processed dielectric materials.[156]

4.8. Electrodes

Inkjet printing of electrodes is, as of today, a large challenge for fully inkjet-printed devices. Due to particular drying conditions encountered in inkjet printing, such as the coffee-ring effect, the surface roughness of printed films is much higher compared to conventional vacuum-processing techniques, such as sputtering.[163] Therefore, stacking of printed layers proves itself to be rather challenging, leading to very rough surfaces on which the electrodes must be printed. This causes a worsening of the contact between electrodes and channel/dielectric, leading to higher contact resistance and higher threshold voltages.[163] The repertoire of electrode materials compatible with IGZO channels has expanded significantly in recent years, propelled by rigorous research endeavors in the field. The compatibility of silver, titanium, indium-tin-oxide, fluorene-doped tin-oxide, antimony-tin-oxide, annealed copper-oxide, and molybdenum-oxide with IGZO channels has been thoroughly investigated, with findings indicating that silver is particularly well-suited for IGZO TFT electrodes, due to the adequate work function.[164–168] More recently, the use of graphene has proven to be viable for IGZO TFT electrodes, boasting high performance and good interaction with the channel layer.[67,77]

© 2024 The Author(s). Advanced Electronic Materials published by Wiley-VCH GmbH

2199160x, 0, Downloaded from https://onlinelibrary.wiley.com/doi/10.1002/aelm.202400478 by Karlsruher Institut F., Wiley Online Library on [10/1/2024]. See the Terms and Conditions (https://onlinelibrary.wiley.com/terms-and-conditions) on Wiley Online Library for rules of use; OA articles are governed by the applicable Creative Commons License

4.8.1. Silver Electrodes

Silver, renowned for its exceptional conductivity and anti-oxidation properties, emerges as an optimal choice for various applications, including TFT electrodes.[169–172] Inkjet printing of silver electrodes onto IGZO substrates commenced several years thereafter, employing either nanoparticle-based or salt precursor-based ink synthesis routes. Notably, a primary challenge associated with silver nanoparticle inks lies in the presence of organic constituents necessitated for nanoparticle precipitation prior to ink synthesis. These cause contact problems between the channel material and the silver electrodes.[173] Investigations have revealed that partial removal of organic compounds from the ink can be achieved through substrate heating, facilitating the merging and diffusion of silver nanoparticles into the IGZO channel layer (see Figure 9b,c).[174] Similarly, a comparative analysis between IGZO TFTs fabricated using nanoparticle-based and salt precursor-based inks demonstrated superior device characteristics in the latter case (see Figure 9d,e),[173] underscoring the potential of salt precursor-based inks in advancing inkjet-printed IGZO device performance. Moreover, investigations have revealed that augmenting the thickness of the IGZO layer correlates with diminished contact resistance. This phenomenon likely arises from heightened surface roughness accompanying the increase in layer thickness, thereby enhancing the contact profile. Notably, devices fabricated with a channel thickness of ≈80 nm exhibited properties akin to those observed in devices featuring sputtered silver electrodes.[175]

4.8.2. Graphene Electrodes

Graphene, as an electrode material, represents a burgeoning research domain that has already demonstrated its viability as a promising alternative to silver electrodes, primarily attributed to the improved electrical contact formation observed between graphene electrodes and indium gallium zinc oxide (IGZO) channels compared to silver electrodes.[77] Various carbon-based electrodes have exhibited efficacy in conjunction with both IGZO and indium oxide materials.[176–179] The advent of novel graphene ink synthesis methodologies has facilitated the inkjet printing of graphene electrodes, marking a significant advancement in the field.[180–184] Secor et al. showcased the favorable interaction between graphene electrodes and IGZO channels, culminating in the fabrication of functional middle-contact devices characterized by superior electrical properties, reduced hysteresis behavior, and both long-term and high-temperature stability (see Figure 9f).[77] Furthermore, recent advancements have led to the demonstration of fully inkjet-printed IGZO Schottky barrier transistors featuring reduced graphene oxide (rGO) electrodes, thereby reaffirming the compatibility and efficacy of graphene in tandem with IGZO for transistor devices.[67]

4.8.3. Fully Inkjet-Printed IGZO TFTs

To the best of our knowledge, only one scholarly publication has thus far addressed the fabrication of fully inkjet-printed indium gallium zinc oxide (IGZO) thin-film transistors (TFTs). Arjmandi et al. conducted this study wherein the devices were constructed on an aluminum substrate, featuring an aluminum oxide (Al_2O_3) dielectric layer and silver electrodes.[68] A schematic of the device can be found in Figure 9g. The aluminum substrate, serving as the gate electrode, underwent meticulous cleaning using trichloroethylene (TCE) and isopropyl alcohol (IPA) followed by polishing. Subsequently, the gate oxide was generated through substrate oxidation via inkjet-printed solution deposition. To accomplish this, a solution comprising NH_4OH:H_2O_2:H_2O was synthesized and directly inkjet-printed onto the substrate, followed by a 10-min heating process at 60 °C. Following the inkjet printing of the IGZO film atop the gate oxide, the devices underwent annealing at 240 °C for 45 min. Finally, silver electrodes were inkjet-printed onto the IGZO film and subjected to sintering at 130 °C for 20 min. The IGZO films exhibited thicknesses ranging between 50 and 70 nm, with a hall mobility of 2.2 cm^2 V^{-1} s^{-1} and a threshold voltage falling within the range of 4–6 V.[68]

The challenges outlined in this chapter highlight the inherent complexities in achieving a fully inkjet-printed IGZO transistor. The development of appropriate deposition techniques and ink formulations that facilitate the printing of smooth, thin dielectric layers, as well as low-resistance metal contacts, remains a significant and time-intensive task. Numerous research teams globally are dedicated to addressing these obstacles, aiming to establish a scalable, high-yield process for the full inkjet-based fabrication of IGZO transistors.

5. Conclusions

In conclusion, this review has offered a comprehensive overview of past research endeavors concerning inkjet printing methodologies for IGZO TFTs. We have examined the synthesis routes available for IGZO inks, elucidated their unique characteristics, and delineated the essential printing prerequisites and optimization strategies. Furthermore, we have explored various possibilities regarding inkjet-printed electrodes and dielectric materials tailored for fully inkjet-printed IGZO TFTs.

While our review has showcased only a singular fully inkjet-printed device, it is evident that considerable opportunities for the fabrication of high-performance inkjet-printed devices remain untapped. The significance of this endeavor cannot be overstated, particularly given the growing interest in solution-processed TFTs due to their cost-effectiveness and compatibility with flexible, biodegradable electronics, transparent display technologies, and lightweight portable devices. Additionally, considering the superior mobility, stability, and light transmittance characteristics exhibited by IGZO, it becomes apparent that fully inkjet-printed IGZO TFTs hold significant potential to drive innovative advancements in future technologies, facilitating the development of revolutionary low-cost products. We hope that this subject will be explored even further in future research, as many facets remain unexplored. Doping of IGZO up to high-entropy variations that include even more precursor metals could enable undiscovered properties or even more precise tuning, whereas new IGZO ink formulations, coupled with advancements in inkjet-printing technology, could enable higher device density, and faster electronics and therefore open up a range of new

© 2024 The Author(s). Advanced Electronic Materials published by Wiley-VCH GmbH

2199160x, 0, Downloaded from https://onlinelibrary.wiley.com/doi/10.1002/aelm.202400478 by Karlsruher Institut F., Wiley Online Library on [10/1/2024]. See the Terms and Conditions (https://onlinelibrary.wiley.com/terms-and-conditions) on Wiley Online Library for rules of use; OA articles are governed by the applicable Creative Commons License

possible applications for cheap, solution-processed, and transparent devices based on IGZO channels.

Acknowledgements

J.A.-H. acknowledges funding by the DFG under Germany's Excellence Strategy via the Excellence Cluster "3D Matter Made to Order" (EXC-2082/1-390761711). J.A.-H. and B.B. acknowledge financial support from the KIT via the project Auto.MAP and the Helmholtz Program "Materials Systems Engineering" under program no. 43.31.01.

Conflict of Interest

The authors declare no conflict of interest.

Data Availability Statement

Data sharing does not apply to this article as no new data was created or analyzed in this study.

Keywords

IGZO, inkjet printing, TFTs

Received: June 18, 2024
Revised: September 19, 2024
Published online:

[1] J. F. Wager, *Science* **2003**, *300*, 1245.
[2] J. F. Wager, *Inf. Disp.* **2014**, *30*, 26.
[3] T. Kamiya, K. Nomura, H. Hosono, *Sci. Technol. Adv. Mater.* **2010**, *11*, 044305.
[4] J. S. Park, W.-J. Maeng, H.-S. Kim, J.-S. Park, *Thin Solid Films* **2012**, *520*, 1679.
[5] S. J. Kim, S. Yoon, H. J. Kim, *Jpn. J. Appl. Phys.* **2014**, *53*, 02BA02.
[6] S. R. Thomas, P. Pattanasattayavong, T. D. Anthopoulos, *Chem. Soc. Rev.* **2013**, *42*, 6910.
[7] Y. Chen, K. Denis, P. Kazlas, P. Drzaic, *SID Symp. Dig. Tech. Pap.* **2001**, *32*, 157.
[8] J.-J. Lih, C.-F. Sung, C.-H. Li, T.-H. Hsiao, H.-H. Lee, *J. Soc. Inf. Disp.* **2004**, *12*, 367.
[9] Y. He, R. Hattori, J. Kanicki, *IEEE Electron Device Lett.* **2000**, *21*, 590.
[10] A. Nathan, G. R. Chaji, S. J. Ashtiani, *J. Disp. Technol.* **2005**, *1*, 267.
[11] G. W. Shim, W. Hong, J.-H. Cha, J. H. Park, K. J. Lee, S.-Y. Choi, *Adv. Mater.* **2020**, *32*, 1907166.
[12] Y. G. Mo, M. Kim, C. K. Kang, J. H. Jeong, Y. S. Park, C. G. Choi, H. D. Kim, S. S. Kim, *SID Symp. Dig. Tech. Pap.* **2010**, *41*, 1037.
[13] J. Nishii, F. M. Hossain, S. Takagi, T. Aita, K. Saikusa, Y. Ohmaki, I. Ohkubo, S. Kishimoto, A. Ohtomo, T. Fukumura, F. Matsukura, Y. Ohno, H. Koinuma, H. Ohno, M. Kawasaki, *Jpn. J. Appl. Phys.* **2003**, *42*, L347.
[14] K. Lee, J. H. Kim, S. Im, *Appl. Phys. Lett.* **2006**, *88*, 023504.
[15] B. J. Norris, J. Anderson, J. F. Wager, D. A. Keszler, *J. Phys. Appl. Phys.* **2003**, *36*, L105.
[16] S. Masuda, K. Kitamura, Y. Okumura, S. Miyatake, H. Tabata, T. Kawai, *J. Appl. Phys.* **2003**, *93*, 1624.
[17] H. S. Bae, S. Im, *Thin Solid Films* **2004**, *469*, 75.
[18] P. Barquinha, A. Pimentel, A. Marques, L. Pereira, R. Martins, E. Fortunato, *J. Non-Cryst. Solids* **2006**, *352*, 1749.
[19] Y.-L. Wang, F. Ren, W. Lim, D. P. Norton, S. J. Pearton, I. I. Kravchenko, J. M. Zavada, *Appl. Phys. Lett.* **2007**, *90*, 232103.
[20] E. Fortunato, P. Barquinha, A. Pimentel, L. Pereira, G. Gonçalves, R. Martins, *Phys. Status Solidi RRL – Rapid Res. Lett.* **2007**, *1*, R34.
[21] T. Miyasako, M. Senoo, E. Tokumitsu, *Appl. Phys. Lett.* **2005**, *86*, 162902.
[22] L. Wang, M.-H. Yoon, G. Lu, Y. Yang, A. Facchetti, T. J. Marks, *Nat. Mater.* **2006**, *5*, 893.
[23] K. Nomura, H. Ohta, K. Ueda, T. Kamiya, M. Hirano, H. Hosono, *Science* **2003**, *300*, 1269.
[24] J. Yoon, G.-Y. Bae, S. Yoo, J. I. Yoo, N.-H. You, W.-K. Hong, H. C. Ko, *J. Alloys Compd.* **2020**, *817*, 152788.
[25] C. M. Yang, J. C. Wang, T. W. Chiang, Y. T. Lin, T. W. Juan, T. G. Chen, M. Y. Shih, C. E. Lue, C. S. Lai, *Int. J. Nanotechnol.* **2014**, *11*, 15.
[26] J.-Y. Pyo, W.-J. Cho, *Sens. Actuators, B* **2018**, *276*, 101.
[27] N. Kumar, J. Kumar, S. Panda, *AIP Adv.* **2015**, *5*, 067123.
[28] A. Chasin, L. Zhang, A. Bhoolokam, M. Nag, S. Steudel, B. Govoreanu, G. Gielen, P. Heremans, *IEEE Electron Device Lett.* **2014**, *35*, 642.
[29] J. Y. Bak, M.-K. Ryu, S. H. K. Park, C.-S. Hwang, S. M. Yoon, *IEEE Trans. Electron Devices* **2014**, *61*, 2404.
[30] H. Inoue, T. Matsuzaki, S. Nagatsuka, Y. Okazaki, T. Sasaki, K. Noda, D. Matsubayashi, T. Ishizu, T. Onuki, A. Isobe, Y. Shionoiri, K. Kato, T. Okuda, J. Koyama, S. Yamazaki, *IEEE J. Solid-State Circuits* **2012**, *47*, 2258.
[31] R. A. Martins, E. Carlos, J. Deuermeier, M. E. Pereira, R. Martins, E. Fortunato, A. Kiazadeh, *J. Mater. Chem. C* **2022**, *10*, 1991.
[32] J. Rosa, A. Kiazadeh, L. Santos, J. Deuermeier, R. Martins, H. L. Gomes, E. Fortunato, *ACS Omega* **2017**, *2*, 8366.
[33] M. E. Pereira, J. Deuermeier, P. Freitas, P. Barquinha, W. Zhang, R. Martins, E. Fortunato, A. Kiazadeh, *APL Mater.* **2022**, *10*, 011113.
[34] K. Nomura, H. Ohta, A. Takagi, T. Kamiya, M. Hirano, H. Hosono, *Nature* **2004**, *432*, 488.
[35] D. Mitzi, *Solution Processing of Inorganic Materials*, John Wiley & Sons, Hoboken, New Jersey **2008**.
[36] G. Cadilha Marques, L. Yang, Y. Liu, V. Wollersen, T. Scherer, B. Breitung, M. Wegener, J. Aghassi-Hagmann, *Adv. Mater. Technol.* **2023**, *8*, 2300893.
[37] N. Hussain, T. Fu, G. Marques, C. Das, T. Scherer, U. Bog, L. Berner, I. Wacker, R. R. Schröder, J. Aghassi-Hagmann, M. Hirtz, *Adv. Mater. Technol.* **2021**, *6*, 2100650.
[38] S. A. Singaraju, G. C. Marques, P. Gruber, R. Kruk, H. Hahn, B. Breitung, J. Aghassi-Hagmann, *Phys. Status Solidi RRL – Rapid Res. Lett.* **2020**, *14*, 2000252.
[39] H.-C. Cheng, C.-F. Chen, C.-C. Lee, *Thin Solid Films* **2006**, *498*, 142.
[40] J. W. Hennek, Y. Xia, K. Everaerts, M. C. Hersam, A. Facchetti, T. J. Marks, *ACS Appl. Mater. Interfaces* **2012**, *4*, 1614.
[41] D. Kim, Y. Jeong, C. Y. Koo, K. Song, J. Moon, *Jpn. J. Appl. Phys.* **2010**, *49*, 05EB06.
[42] G. H. Kim, H. S. Kim, H. S. Shin, B. D. Ahn, K. H. Kim, H. J. Kim, *Thin Solid Films* **2009**, *517*, 4007.
[43] H. S. Kim, M.-G. Kim, Y.-G. Ha, M. G. Kanatzidis, T. J. Marks, A. Facchetti, *J. Am. Chem. Soc.* **2009**, *131*, 10826.
[44] M.-G. Kim, H. S. Kim, Y.-G. Ha, J. He, M. G. Kanatzidis, A. Facchetti, T. J. Marks, *J. Am. Chem. Soc.* **2010**, *132*, 10352.
[45] D.-H. Lee, Y.-J. Chang, G. S. Herman, C.-H. Chang, *Adv. Mater.* **2007**, *19*, 843.
[46] J. A. Letizia, S. Cronin, R. P. Ortiz, A. Facchetti, M. A. Ratner, T. J. Marks, *Chem. – Eur. J.* **2010**, *16*, 1911.
[47] A. Nadarajah, M. Z. B. Wu, K. Archila, M. G. Kast, A. M. Smith, T. H. Chiang, D. A. Keszler, J. F. Wager, S. W. Boettcher, *Chem. Mater.* **2015**, *27*, 5587.
[48] J. J. Schneider, R. C. Hoffmann, J. Engstler, O. Soffke, W. Jaegermann, A. Issanin, A. Klyszcz, *Adv. Mater.* **2008**, *20*, 3383.

© 2024 The Author(s). Advanced Electronic Materials published by Wiley-VCH GmbH

2199160x, 0, Downloaded from https://onlinelibrary.wiley.com/doi/10.1002/aelm.202400478 by Karlsruher Institut F., Wiley Online Library on [10/11/2024]. See the Terms and Conditions (https://onlinelibrary.wiley.com/terms-and-conditions) on Wiley Online Library for rules of use; OA articles are governed by the applicable Creative Commons License

[49] Y. Wang, X. W. Sun, G. K. L. Goh, H. V. Demir, H. Y. Yu, *IEEE Trans. Electron Devices* **2011**, *58*, 480.
[50] F. Liu, L. Gillan, J. Leppäniemi, A. Alastalo, *Adv. Mater. Interfaces* **2023**, *10*, 2202258.
[51] C.-H. Chang, Y.-J. Chang, D.-H. Lee, *Solution Deposition of Inorganic Materials and Electronic Devices Made Comprising the Inorganic Materials*, **2006**, p. 8679587.
[52] S.-Y. Han, D.-H. Lee, G. S. Herman, C.-H. Chang, *J. Disp. Technol.* **2009**, *5*, 520.
[53] D.-H. Lee, S.-Y. Han, G. S. Herman, C. Chang, *J. Mater. Chem.* **2009**, *19*, 3135.
[54] H. Hosono, M. Yasukawa, H. Kawazoe, *J. Non-Cryst. Solids* **1996**, *203*, 334.
[55] H. Hosono, N. Kikuchi, N. Ueda, H. Kawazoe, *J. Non-Cryst. Solids* **1996**, *198–200*, 165.
[56] T. Kamiya, K. Nomura, H. Hosono, *J. Disp. Technol.* **2009**, *5*, 273.
[57] H. Li, Y. Guo, J. Robertson, *Phys. Rev. Mater.* **2018**, *2*, 074601.
[58] E. Fortunato, P. Barquinha, R. Martins, *Adv. Mater.* **2012**, *24*, 2945.
[59] J.-S. Park, H. Kim, I.-D. Kim, *J. Electroceram.* **2014**, *32*, 117.
[60] Y. K. Shen, Z. Liu, X. L. Wang, W. K. Ma, Z. H. Chen, T. P. Chen, H. Y. Zhang, *Solid-State Electron.* **2017**, *138*, 108.
[61] H. Hosono, *J. Non-Cryst. Solids* **2006**, *352*, 851.
[62] J. K. Jeong, J. H. Jeong, H. W. Yang, J.-S. Park, Y.-G. Mo, H. D. Kim, *Appl. Phys. Lett.* **2007**, *91*, 113505.
[63] M. Moreira, E. Carlos, C. Dias, J. Deuermeier, M. Pereira, P. Barquinha, R. Branquinho, R. Martins, E. Fortunato, *Nanomaterials* **2019**, *9*, 1273.
[64] L. Nayak, S. Mohanty, S. K. Nayak, A. Ramadoss, *J. Mater. Chem. C* **2019**, *7*, 8771.
[65] E. Carlos, R. Martins, E. Fortunato, R. Branquinho, *Chem. – Eur. J.* **2020**, *26*, 9099.
[66] S. Jeong, J.-Y. Lee, S. S. Lee, S.-W. Oh, H. H. Lee, Y.-H. Seo, B.-H. Ryu, Y. Choi, *J. Mater. Chem.* **2011**, *21*, 17066.
[67] D. U. Lim, S. Choi, S. Kim, Y. J. Choi, S. Lee, M. S. Kang, Y.-H. Kim, J. H. Cho, *ACS Nano* **2019**, *13*, 8213.
[68] N. Arjmandi, M. Seraj, M. Najafi, S. A. R. A. Afshar, in *2021 IEEE 16th Nanotechnol. Mater. Devices Conf. NMDC*, IEEE, Vancouver, BC, Canada **2021**, pp. 1–4.
[69] M. Xie, S. Wu, Z. Chen, Q. Khan, X. Wu, S. Shao, Z. Cui, *RSC Adv.* **2016**, *6*, 41439.
[70] K. Liang, Y. Wang, S. Shao, M. Luo, V. Pecunia, L. Shao, J. Zhao, Z. Chen, L. Mo, Z. Cui, *J. Mater. Chem. C* **2019**, *7*, 6169.
[71] S. Wu, Q. Zhang, Z. Chen, L. Mo, S. Shao, Z. Cui, *J. Mater. Chem. C* **2017**, *5*, 7495.
[72] Q. Luo, in *Solution Processed Metal Oxide Thin Films for Electronic Applications*, Elsevier, Amsterdam, Netherlands, **2020**, pp. 63–82.
[73] M.-C. Wu, K.-C. Hsiao, H.-C. Lu, *Mater. Chem. Phys.* **2015**, *162*, 386.
[74] N. Fukuda, Y. Watanabe, S. Uemura, Y. Yoshida, T. Nakamura, H. Ushijima, *J. Mater. Chem. C* **2014**, *2*, 2448.
[75] C. Jeffrey Brinker, G. W. Scherer, in *Sol-Gel Science*, Elsevier, Amsterdam, Netherlands, **1990**.
[76] Y. Choi, G. H. Kim, W. H. Jeong, H. J. Kim, B. D. Chin, J.-W. Yu, *Thin Solid Films* **2010**, *518*, 6249.
[77] E. B. Secor, J. Smith, T. J. Marks, M. C. Hersam, *ACS Appl. Mater. Interfaces* **2016**, *8*, 17428.
[78] K. Everaerts, L. Zeng, J. W. Hennek, D. I. Camacho, D. Jariwala, M. J. Bedzyk, M. C. Hersam, T. J. Marks, *ACS Appl. Mater. Interfaces* **2013**, *5*, 11884.
[79] G. Rajbhandari, P. W. Vanaraj, B. B. Maskey, H. Park, A. Sapkota, Y. Jung, Y. Majima, G. Cho, *Adv. Electron. Mater.* **2018**, *4*, 1800078.
[80] L. Zhang, Q. Guo, Q. Tan, Z. Fan, J. Xiong, *IEEE Access* **2019**, *7*, 184312.
[81] N. Aboualigaledari, M. Rahmani, *J. Compos. Compd.* **2021**, *3*, 25.
[82] E. Carlos, R. Branquinho, A. Kiazadeh, P. Barquinha, R. Martins, E. Fortunato, *ACS Appl. Mater. Interfaces* **2016**, *8*, 31100.
[83] M.-G. Kim, M. G. Kanatzidis, A. Facchetti, T. J. Marks, *Nat. Mater.* **2011**, *10*, 382.
[84] K. C. Patil, M. S. Hegde, T. Rattan, S. T. Aruna, in *Chemistry of Nanocrystalline Oxide Materials*, World Scientific, Singapore, **2008**, pp. 42–60.
[85] P. K. Nayak, M. N. Hedhili, D. Cha, H. N. Alshareef, *ACS Appl. Mater. Interfaces* **2013**, *5*, 3587.
[86] J. Kim, H.-H. Park, Y.-H. Kim, S. K. Park, *Sci. Adv. Mater.* **2015**, *7*, 1525.
[87] S. Choi, K.-T. Kim, S. K. Park, Y.-H. Kim, *Materials* **2019**, *12*, 852.
[88] S. Hwang, J. H. Lee, C. H. Woo, J. Y. Lee, H. K. Cho, *Thin Solid Films* **2011**, *519*, 5146.
[89] Y. Wang, S. W. Liu, X. W. Sun, J. L. Zhao, G. K. L. Goh, Q. V. Vu, H. Y. Yu, *J. Sol-Gel Sci. Technol.* **2010**, *55*, 322.
[90] C.-Y. Tsay, T.-Y. Yan, *J. Phys. Chem. Solids* **2014**, *75*, 142.
[91] X. Wang, Z. Shen, J. Li, S. Wu, *Membranes* **2021**, *11*, 134.
[92] S.-Y. Han, G. S. Herman, C. Chang, *J. Am. Chem. Soc.* **2011**, *133*, 5166.
[93] L.-F. Teng, P.-T. Liu, Y.-J. Lo, Y.-J. Lee, *Appl. Phys. Lett.* **2012**, *101*, 132901.
[94] T. Jun, K. Song, Y. Jeong, K. Woo, D. Kim, C. Bae, J. Moon, *J. Mater. Chem.* **2011**, *21*, 1102.
[95] Y.-H. Kim, J.-S. Heo, T.-H. Kim, S. Park, M.-H. Yoon, J. Kim, M. S. Oh, G.-R. Yi, Y.-Y. Noh, S. K. Park, *Nature* **2012**, *489*, 128.
[96] Y. Seung Rim, W. Hee Jeong, D. Lim Kim, H. Soo Lim, K. Min Kim, H. Jae Kim, *J. Mater. Chem.* **2012**, *22*, 12491.
[97] G. Xia, Q. Zhang, S. Wang, *IEEE Electron Device Lett.* **2018**, *39*, 1868.
[98] C.-H. Choi, S.-Y. Han, Y.-W. Su, Z. Fang, L.-Y. Lin, C.-C. Cheng, C. Chang, *J. Mater. Chem. C* **2015**, *3*, 854.
[99] X. Yu, N. Zhou, J. Smith, H. Lin, K. Stallings, J. Yu, T. J. Marks, A. Facchetti, *ACS Appl. Mater. Interfaces* **2013**, *5*, 7983.
[100] H. Huang, H. Hu, J. Zhu, T. Guo, *J. Electron. Mater.* **2017**, *46*, 4497.
[101] K.-S. Kim, S.-W. Lee, S.-M. Oh, W.-J. Cho, *Mater. Sci. Eng., B* **2013**, *178*, 811.
[102] C.-Y. Chung, B. Zhu, D. G. Ast, R. G. Greene, M. O. Thompson, *Appl. Phys. Lett.* **2015**, *106*, 123506.
[103] Y.-H. Yang, S. S. Yang, K.-S. Chou, *IEEE Electron Device Lett.* **2010**, *31*, 969.
[104] C.-Y. Tsay, T.-T. Huang, *Mater. Chem. Phys.* **2013**, *140*, 365.
[105] Y. S. Rim, D. L. Kim, W. H. Jeong, H. S. Shin, H. J. Kim, *SID Symp. Dig. Tech. Pap.* **2011**, *42*, 1148.
[106] S. Svanberg, in *Atomic and Molecular Spectroscopy*, Springer, Berlin, Heidelberg **2004**, pp. 5–30.
[107] H. Pu, Q. Zhou, L. Yue, Q. Zhang, *Semicond. Sci. Technol.* **2013**, *28*, 105002.
[108] Q. Zhang, C. Ruan, G. Xia, H. Gong, S. Wang, *Thin Solid Films* **2021**, *723*, 138594.
[109] J.-H. Jeon, W.-J. Cho, *Semicond. Sci. Technol.* **2019**, *34*, 015006.
[110] H. J. Cheong, N. Fukuda, H. Sakai, S. Ogura, K. Takeuchi, R. Nagahata, S. Uemura, *Jpn. J. Appl. Phys.* **2014**, *53*, 05HA12.
[111] H. Cheong, S. Ogura, H. Ushijima, M. Yoshida, N. Fukuda, S. Uemura, *AIP Adv.* **2015**, *5*, 067127.
[112] B.-Y. Su, S.-Y. Chu, Y.-D. Juang, H.-C. Chen, *Appl. Phys. Lett.* **2013**, *102*, 192101.
[113] P. K. Nayak, M. N. Hedhili, D. Cha, H. N. Alshareef, *Appl. Phys. Lett.* **2012**, *100*, 202106.
[114] R. D. Deegan, O. Bakajin, T. F. Dupont, G. Huber, S. R. Nagel, T. A. Witten, *Nature* **1997**, *389*, 827.
[115] R. D. Deegan, O. Bakajin, T. F. Dupont, G. Huber, S. R. Nagel, T. A. Witten, *Phys. Rev. E* **2000**, *62*, 756.
[116] M. Kuang, L. Wang, Y. Song, *Adv. Mater.* **2014**, *26*, 6950.

© 2024 The Author(s). Advanced Electronic Materials published by Wiley-VCH GmbH

2199160x, 0, Downloaded from https://onlinelibrary.wiley.com/doi/10.1002/aelm.202400478 by Karlsruher Institut F., Wiley Online Library on [10/11/2024]. See the Terms and Conditions (https://onlinelibrary.wiley.com/terms-and-conditions) on Wiley Online Library for rules of use; OA articles are governed by the applicable Creative Commons License

[117] D. Kim, Y. Jeong, K. Song, S.-K. Park, G. Cao, J. Moon, *Langmuir* **2009**, *25*, 11149.
[118] K.-J. Baeg, D. Khim, J.-H. Kim, M. Kang, I.-K. You, D.-Y. Kim, Y.-Y. Noh, *Org. Electron.* **2011**, *12*, 634.
[119] S. Magdassi, in The Chemistry Of Inkjet Inks, World Scientific, **2009**, pp. 19–41.
[120] J. Sun, B. Bao, M. He, H. Zhou, Y. Song, *ACS Appl. Mater. Interfaces* **2015**, *7*, 28086.
[121] M. J. Rosen, *Surfactants and Interfacial Phenomena*, Wiley, Hoboken, New Jersey **2004**.
[122] R. M. Podhajny, in *Surf. Phenom. Fine Part. Water-Based Coat. Print. Technol*, (Eds.: M. K. Sharma, F. J. Micale), Springer US, Boston, MA **1991**, pp. 41–58.
[123] D. Zhou, B. Li, H. Wang, Y. Peng, J. Zhao, M. Salik, L. Yi, X. Zhang, Y. Wang, *J. Alloys Compd.* **2015**, *648*, 587.
[124] C. Avis, H. R. Hwang, J. Jang, *ACS Appl. Mater. Interfaces* **2014**, *6*, 10941.
[125] A. Lee, K. Sudau, K. H. Ahn, S. J. Lee, N. Willenbacher, *Ind. Eng. Chem. Res.* **2012**, *51*, 13195.
[126] D. Xie, H. Wu, A. Zaccone, L. Braun, H. Chen, M. Morbidelli, *Soft Matter* **2010**, *6*, 2692.
[127] A. Zaccone, H. Wu, D. Gentili, M. Morbidelli, *Phys. Rev. E* **2009**, *80*, 051404.
[128] A. Zaccone, D. Gentili, H. (吴华) Wu, M. Morbidelli, *J. Chem. Phys.* **2010**, *132*, 134903.
[129] V. Ramachandran, H. S. Fogler, *J. Fluid Mech.* **1999**, *385*, 129.
[130] H. M. Wyss, D. L. Blair, J. F. Morris, H. A. Stone, D. A. Weitz, *Phys. Rev. E* **2006**, *74*, 061402.
[131] S. Fathi, P. Dickens, *J. Mater. Process. Technol.* **2013**, *213*, 383.
[132] X. Yan, K. Shi, X. Chu, F. Yang, Y. Chi, X. Yang, *Coatings* **2019**, *9*, 619.
[133] Y. S. Rim, H. Chen, X. Kou, H.-S. Duan, H. Zhou, M. Cai, H. J. Kim, Y. Yang, *Adv. Mater.* **2014**, *26*, 4273.
[134] S. Shao, K. Liang, X. Li, J. Zhang, C. Liu, Z. Cui, J. Zhao, *J. Mater. Sci. Technol.* **2021**, *81*, 26.
[135] N. Tiwari, R. Narayan Chauhan, P.-T. Liu, H.-P. D. Shieh, *RSC Adv.* **2016**, *6*, 75693.
[136] A. Liu, H. Zhu, H. Sun, Y. Xu, Y.-Y. Noh, *Adv. Mater.* **2018**, *30*, 1706364.
[137] W. Cai, H. Ning, Z. Zhu, J. Wei, S. Zhou, R. Yao, Z. Fang, X. Huang, X. Lu, J. Peng, *Nanoscale Res. Lett.* **2019**, *14*, 80.
[138] N. Graddage, T.-Y. Chu, H. Ding, C. Py, A. Dadvand, Y. Tao, *Org. Electron.* **2016**, *29*, 114.
[139] L. Gillan, S. Li, J. Lahtinen, C.-H. Chang, A. Alastalo, J. Leppäniemi, *Adv. Mater. Interfaces* **2021**, *8*, 2100728.
[140] W. J. Scheideler, M. W. McPhail, R. Kumar, J. Smith, V. Subramanian, *ACS Appl. Mater. Interfaces* **2018**, *10*, 37277.
[141] J. Jang, H. Kang, H. C. N. Chakravarthula, V. Subramanian, *Adv. Electron. Mater.* **2015**, *1*, 1500086.
[142] Y. Li, L. Lan, S. Sun, Z. Lin, P. Gao, W. Song, E. Song, P. Zhang, J. Peng, *ACS Appl. Mater. Interfaces* **2017**, *9*, 8194.
[143] Z. Zhu, H. Ning, W. Cai, J. Wei, S. Zhou, R. Yao, X. Lu, J. Zhang, Z. Zhou, J. Peng, *Langmuir* **2018**, *34*, 6413.
[144] K. Yim, Y. Yong, J. Lee, K. Lee, H.-H. Nahm, J. Yoo, C. Lee, C. Seong Hwang, S. Han, *NPG Asia Mater.* **2015**, *7*, e190.
[145] W. Yang, K. Song, Y. Jung, S. Jeong, J. Moon, *J. Mater. Chem. C* **2013**, *1*, 4275.
[146] J. Ko, J. Kim, S. Y. Park, E. Lee, K. Kim, K.-H. Lim, Y. S. Kim, *J. Mater. Chem. C* **2014**, *2*, 1050.
[147] S. T. Meyers, J. T. Anderson, D. Hong, C. M. Hung, J. F. Wager, D. A. Keszler, *Chem. Mater.* **2007**, *19*, 4023.
[148] L. Lu, Y. Miura, T. Nishida, M. Echizen, Y. Ishikawa, K. Uchiyama, Y. Uraoka, *Jpn. J. Appl. Phys.* **2012**, *51*, 03CB05.
[149] K. Banger, C. Warwick, J. Lang, K. Broch, J. E. Halpert, J. Socratous, A. Brown, T. Leedham, H. Sirringhaus, *Chem. Sci.* **2016**, *7*, 6337.
[150] P. N. Plassmeyer, K. Archila, J. F. Wager, C. J. Page, *ACS Appl. Mater. Interfaces* **2015**, *7*, 1678.
[151] Z. Yang, H. Pu, C. Cui, L. Zhang, C. Dong, Q. Zhang, *IEEE Electron Device Lett.* **2014**, *35*, 557.
[152] S. Bolat, P. Fuchs, S. Knobelspies, O. Temel, G. T. Sevilla, E. Gilshtein, C. Andres, I. Shorubalko, Y. Liu, G. Tröster, A. N. Tiwari, Y. E. Romanyuk, *Adv. Electron. Mater.* **2019**, *5*, 1800843.
[153] J. Lee, H. Seul, J. K. Jeong, *J. Alloys Compd.* **2018**, *741*, 1021.
[154] N. Koslowski, V. Trouillet, J. J. Schneider, *J. Mater. Chem. C* **2020**, *8*, 8521.
[155] E. Carlos, R. Branquinho, A. Kiazadeh, J. Martins, P. Barquinha, R. Martins, E. Fortunato, *ACS Appl. Mater. Interfaces* **2017**, *9*, 40428.
[156] S. Zhou, J. Zhang, X. Guo, H. Ning, D. Guo, R. Yao, Z. Zhu, Z. Liang, Z. Fang, J. Peng, *J. Mater. Chem. C* **2020**, *8*, 12578.
[157] S. Dai, Y. Wang, J. Zhang, Y. Zhao, F. Xiao, D. Liu, T. Wang, J. Huang, *ACS Appl. Mater. Interfaces* **2018**, *10*, 39983.
[158] S. Zhang, C. Tang, J. Hao, X. Wang, *Appl. Phys. Lett.* **2017**, *111*, 012902.
[159] D. Gaspar, S. N. Fernandes, A. G. de Oliveira, J. G. Fernandes, P. Grey, R. V. Pontes, L. Pereira, R. Martins, M. H. Godinho, E. Fortunato, *Nanotechnology* **2014**, *25*, 094008.
[160] D. Gaspar, L. Pereira, A. Delattre, D. Guerin, E. Fortunato, R. Martins, *Phys. Status Solidi C* **2015**, *12*, 1421.
[161] I. Cunha, R. Barras, P. Grey, D. Gaspar, E. Fortunato, R. Martins, L. Pereira, *Adv. Funct. Mater.* **2017**, *27*, 1606755.
[162] A. Petritz, A. Wolfberger, A. Fian, T. Griesser, M. Irimia-Vladu, B. Stadlober, *Adv. Mater.* **2015**, *27*, 7645.
[163] R. Tao, H. Ning, J. Chen, J. Zou, Z. Fang, C. Yang, Y. Zhou, J. Zhang, R. Yao, J. Peng, *IEEE J. Electron Devices Soc.* **2018**, *6*, 774.
[164] Y. Ueoka, T. Nishibayashi, Y. Ishikawa, H. Yamazaki, Y. Osada, M. Horita, Y. Uraoka, *Jpn. J. Appl. Phys.* **2014**, *53*, 04EB03.
[165] Y. Ueoka, Y. Ishikawa, J. P. Bermundo, H. Yamazaki, S. Urakawa, Y. Osada, M. Horita, Y. Uraoka, *Jpn. J. Appl. Phys.* **2014**, *53*, 03CC04.
[166] K.-H. Choi, H.-K. Kim, *Appl. Phys. Lett.* **2013**, *102*, 052103.
[167] S. Hu, Z. Fang, H. Ning, R. Tao, X. Liu, Y. Zeng, R. Yao, F. Huang, Z. Li, M. Xu, L. Wang, L. Lan, J. Peng, *Materials* **2016**, *9*, 623.
[168] E. Carlos, R. Branquinho, P. Barquinha, R. Martins, E. Fortunato, in Chem. Solut. Synth. Mater. Des. Thin Film Device Appl, Elsevier, **2021**, pp. 585–621.
[169] R. Tao, H. Ning, Z. Fang, J. Chen, W. Cai, Y. Zhou, Z. Zhu, R. Yao, J. Peng, *J. Phys. Chem. C* **2017**, *121*, 8992.
[170] K. Teng, R. Vest, *IEEE Trans. Compon. Hybrids Manuf. Technol.* **1987**, *10*, 545.
[171] W. Tang, L. Feng, J. Zhao, Q. Cui, S. Chen, X. Guo, *J. Mater. Chem. C* **2014**, *2*, 1995.
[172] S. Gamerith, A. Klug, H. Scheiber, U. Scherf, E. Moderegger, E. J. W. List, *Adv. Funct. Mater.* **2007**, *17*, 3111.
[173] C. Yang, Z. Fang, H. Ning, R. Tao, J. Chen, Y. Zhou, Z. Zheng, R. Yao, L. Wang, J. Peng, Y. Song, *Appl. Sci.* **2017**, *7*, 844.
[174] H. Ning, J. Chen, Z. Fang, R. Tao, W. Cai, R. Yao, S. Hu, Z. Zhu, Y. Zhou, C. Yang, J. Peng, *Materials* **2017**, *10*, 51.
[175] J. Chen, H. Ning, Z. Fang, R. Tao, C. Yang, Y. Zhou, R. Yao, M. Xu, L. Wang, J. Peng, *J. Phys. Appl. Phys.* **2018**, *51*, 165103.
[176] M.-S. Lee, K. Lee, S.-Y. Kim, H. Lee, J. Park, K.-H. Choi, H.-K. Kim, D.-G. Kim, D.-Y. Lee, S. Nam, J.-U. Park, *Nano Lett.* **2013**, *13*, 2814.
[177] S. J. Lee, T. Il Lee, J. H.o Park, I.-K. Oh, H. Kim, J. H. Kim, C.-H. Kim, G. S. Chae, H. K. Baik, J.-M. Myoung, *J. Mater. Chem. C* **2015**, *3*, 1403.
[178] D. Luo, H. Xu, M. Zhao, M. Li, M. Xu, J. Zou, H. Tao, L. Wang, J. Peng, *ACS Appl. Mater. Interfaces* **2015**, *7*, 3633.
[179] J. Eun Lee, B. K. Sharma, S.-K. Lee, H. Jeon, B. Hee Hong, H.-J. Lee, J.-H. Ahn, *Appl. Phys. Lett.* **2013**, *102*, 113112.
[180] E. B. Secor, S. Lim, H. Zhang, C. D. Frisbie, L. F. Francis, M. C. Hersam, *Adv. Mater.* **2014**, *26*, 4533.

© 2024 The Author(s). Advanced Electronic Materials published by Wiley-VCH GmbH

2199160x, 0, Downloaded from https://onlinelibrary.wiley.com/doi/10.1002/aelm.202400478 by Karlsruher Institut F., Wiley Online Library on [10/11/2024]. See the Terms and Conditions (https://onlinelibrary.wiley.com/terms-and-conditions) on Wiley Online Library for rules of use; OA articles are governed by the applicable Creative Commons License

[181] E. B. Secor, P. L. Prabhumirashi, K. Puntambekar, M. L. Geier, M. C. Hersam, *J. Phys. Chem. Lett.* **2013**, *4*, 1347.
[182] E. B. Secor, M. C. Hersam, *J. Phys. Chem. Lett.* **2015**, *6*, 620.
[183] W. J. Hyun, E. B. Secor, M. C. Hersam, C. D. Frisbie, L. F. Francis, *Adv. Mater.* **2015**, *27*, 109.
[184] E. B. Secor, B. Y. Ahn, T. Z. Gao, J. A. Lewis, M. C. Hersam, *Adv. Mater.* **2015**, *27*, 6683.

Lorenzo Magnarin earned his B.Sc. in electrical engineering from the Karlsruhe Institute of Technology (KIT), where he is currently pursuing his M.Sc. in Micro- and Nanotechnology. He is working at the Institute of Nanotechnology (KIT), focusing on IGZO ink synthesis. His research interests include metal oxides, advanced characterization techniques, and functionalization of advanced chemical structures.

Ben Breitung leads the "Nanomaterials for Electronic and Energy Applications" research group within Jasmin Aghassi-Hagmann's Research Unit at the Institute of Nanotechnology (INT), Karlsruhe Institute of Technology (KIT). He earned his PhD from KIT in 2013 before joining the BASF/KIT joint lab BELLA (Battery and Electrochemistry Laboratory). In 2017, he began his habilitation and, in 2022, joined the Research Unit "Electronic Devices and Systems." His research focuses on high-entropy and other complex materials for electronics, medical, and energy applications, as well as high-throughput synthesis, characterization methodologies, and AI-assisted materials development.

Jasmin Aghassi-Hagmann is a full professor at the Institute of Nanotechnology (INT) of the Karlsruhe Institute of Technology (KIT) in the Department of Electrical Engineering and Information Technology. She received her diploma in physics from RWTH Aachen and PhD from KIT, Karlsruhe. She has spent 6 years in R&D in the semiconductor industry, developing advanced CMOS nodes until she rejoined academia in 2013. Her research interests are solution processible materials, 2D and 3D functional printing as well as thin film electronic devices and circuits. She serves in various national and international committees such as topic speaker in the Helmholtz Society Research Program Materials System Engineering, and is a member of several executive editorial boards.

© 2024 The Author(s). Advanced Electronic Materials published by Wiley-VCH GmbH

2199160x, 0, Downloaded from https://onlinelibrary.wiley.com/doi/10.1002/aelm.202400478 by Karlsruher Institut F., Wiley Online Library on [10/11/2024]. See the Terms and Conditions (https://onlinelibrary.wiley.com/terms-and-conditions) on Wiley Online Library for rules of use; OA articles are governed by the applicable Creative Commons License